الجمهورية الجزائرية الديمقراطية الشعبية

PEOPLE'S DEMOCRATIE REPUBLIC OF ALGERIA

MINISTRY OF HIGHER EDUCATION AND SCIENTIFIC RESEARCH

UNIVERSITY OF SAAD DAHLEB BLIDA1

INSTITUTE OF AERONAUTICS AND SPACE STUDIES

MAJOR OF PROPULSION AEROSPACE

IN PARTIEL FULFILLMENT OF THE REQUIREMENTS

FOR THE MASTER

DEGREE OF SCIENCE

A Numerical Simulation of the Flow around an Airfoil under static and Pitching conditions

Presented by:

- BOUZIANE ANES.
- MELAKHSSOU NOURELHOUDA.

Under the supervision of:

- Dr. El HADI KHALI **Supervisor**
- Dr. L.SBAA **Co-supervisor**

College year 2020/2021.

Acknowledgements

In the name of Allah, the Most Merciful, the Most compassionate all praise be to Allah, the Lord of the worlds; and prayers and peace be upon Mohammed His servant and messenger.

We would like to express our sincere gratitude to our thesis supervisor Mr. Khali El Hadi, for his patience, motivation, enthusiasm, and immense knowledge, without his guidance, this thesis would not been accomplished.

Moreover, not forgetting Mr.Lazab Sbaa. He allowed us to realize this work by showing us his confidence and by encouraging us in our work, and especially for having always been with the listening of our problems. We appreciate his time and efforts throughout the duration of our work.

Our deepest thanks also go to all the members of the jury for their acceptance to review and to enrich our work.

Last but not least, our thanks to everyone who, in one way or another, has helped and supported us to complete our thesis.

Dedication

With the experience of my gratitude, I dedicate this modest work to those who, I would never be able to express my sincere love to them.

To man, my precious offer from the god who owes my life, my success and all my respect: my dear father Toufik

To the woman who suffered without letting me suffer, who never said no to my demands and who spared no effort to make me happy: my adorable mother Hafsia

To my dear sisters

Khawla, Aline.

My brothers

Nourelddine, Bilal

Who have continued to advise, encourage and support me throughout my studies. May God protect them and give them luck and happiness.

To my Best friend, my support Mohamed Iheb who has always been there for me helping me and motivating me

To my friends from the university campus that I spent the good and the bad with them

Amel, Amina, Noura, Rafika, Ida and Soumia

Without forgetting my partner Anes for His moral support, his patience and his understanding throughout this project.

Not forgot all the promo of master2 Aerospace of

The year 2020-2021

NouElHouda.

I dedicate this work

To my father

God bless his soul, for earning an honest living for us

To my Mother

A strong and gentle soul who taught me to trust in Allah, believe in hard work and so much could be done with little

To my brother Oussama and my sister Sara for their unconditional support and encouragement to purse my interests

To all my friends who have been so supportive and encouraged the fulfillment of this work

To my best thesis, partner NourelHouda

To all those who helped me during my studies believed in me and pried for my success

Not forgot all the promo of master2 Aerospace of

The year 2016-2017

Anes

Abstract

This work presents the Workbench19.0 CFD analysis of static airfoil and OpenFOAM 8.0 CFD analysis of oscillating rotation airfoil. Unsteady subsonic flow is simulated for pitching airfoil at Mach number 0.045 and Reynolds number10.65×10^5. Turbulent effects are also considered for this study by using K-ω SST turbulent model. Two-dimensional unsteady incompressible Navier-Stokes code including two-equation turbulence model. We have not only focused on the active flow control but also analyzed the important parameter reduced frequency at different values; those are 0.1, 0.2 and 0.3. Reduced frequency (κ) is very important parameter of an airfoil in the unsteady motion.

The simulated oscillating Rotation results are compared with the available experimental data. The results have a good agreement with the experimental data. Aerodynamic characteristics during oscillating Rotation have been studied and validated.

Résumé

Ce travail présente l'analyse Workbench19.0 un statique profile et OpenFOAM CFD d'une rotation oscillante profile. Un écoulement subsonique instable est simulé pour une tangage profile au nombre de Mach 0,045 et au nombre de Reynolds 10,65 × 105. Les effets turbulents sont également pris en compte pour cette étude en utilisant le modèle turbulent K-ω SST. Navier-Stokes incompressible instationnaire bidimensionnel incluant un modèle de turbulence à deux équations. Nous sommes non seulement concentrés sur le contrôle de flux actif, mais nous avons également analysé le paramètre important fréquence réduite à différentes valeurs ; ce sont 0,1, 0,2 et 0,3. La fréquence réduite (κ) est un paramètre très important d'un profil aérodynamique dans le mouvement instable.

Les résultats de la Rotation oscillante simulée sont comparés aux données expérimentales disponibles. Les résultats sont similaires aux données expérimentales. Les caractéristiques aérodynamiques lors de la rotation oscillante ont été étudiées et validées.

ملخص

يقدم هذا العمل تحليل Workbench19.0 CFD للجناح الهوائي الثابت وتحليل OpenFOAM 8.0 CFD لجناح الدوران المتأرجح. يتم محاكاة التدفق دون سرعة الصوت غير المستقر لإخراج الجنيح عند رقم ماخ 0.045 ورقم رينولدز 10.65 × 105. تم أخذ التأثيرات المضطربة في الاعتبار أيضًا لهذه الدراسة باستخدام نموذج K-ω SST المضطرب. كود Navier-Stokes غير المستقر ثنائي الأبعاد غير القابل للضغط بما في ذلك نموذج الاضطراب ثنائي المعادلة. لم نركز فقط على التحكم في التدفق النشط ولكننا قمنا أيضًا بتحليل المعلمة المهمة لتقليل التردد عند قيم مختلفة؛ تلك هي 0.1 و 0.2 و 0.3. التردد المنخفض (κ) هو معلمة مهمة جدًا للجنيح في الحركة غير المستقرة.

تمت مقارنة نتائج محاكاة الدوران المتذبذب مع البيانات التجريبية المتوفرة. النتائج تتوافق بشكل جيد مع البيانات التجريبية. تمت دراسة الخصائص الديناميكية الهوائية أثناء الدوران المتذبذب والتحقق من صحتها.

Notations and Acronyms

Some symbols have more than one definition. In the report, it is given by context which definition is used.

α Angle of attack

δ_{ij} The Kronecker delta, δ_{ij} = 1 for i = j and δ_{ij} = 0 otherwise

γ Intermittency

μ Kinematic viscosity

μ_t Eddy viscosity

μ_τ Friction velocity

ν Dynamic viscosity

ω Oscillation frequency, 2πf

ρ Fluid density

τ_{ij} Specific Reynolds stress tensor

τ Stress tensor

F Force vector

g Gravity

r Spatial displacment vector

v Velocity vector

a Oscillation amplitude

C Airfoil Chord length

C_{Pressure} Pressure coefficient

C_D Drag coefficient

C_L Lift coefficient

C_T Thrust coefficient

D Drag

f Oscillation frequency

h Non-dimensional amplitude

k Reduced frequency

k The thermal conductivity coefficient

L Characteristic length

L Lift

l_0 Length scale

p Pressure

p_0 Free stream pressure

Re Reynolds number

$Re_{x,\,\mathrm{crit}}$ Critical Reynolds number for stable laminar flow

T Oscillation period

t Thickness for NACA 00XX series

t Time

U Characteristic velocity

u Velocity component

U_0 Free stream velocity

v Velocity component

v_0 Velocity scale

x, y Cartesian coordinates

BC Boundary condition

BL Boundary layer

CFD Computational fluid dynamics

CV Control volume

DNS Direct numerical simulation

LES Large eddy simulation

LEV Leading edge vortex

MAV Micro air vehicle

RANS Reynolds averaged Navier-Stokes

URANS Unsteady Reynolds averaged Navier-Stokes

Contents

Acknowledgements II

Dedication III

Notations and Acronyms VI

Introduction 1

Chapter I. Generalities on flows around an airfoil 4

I.1 Introduction: 4

I.2 Wings and airfoil: 4

I.2.1 Wing geometry: 4

I.2.2 Airfoils 5

I.3 Aerodynamic Force and Moment 7

I.3.1 Lift 8

I.3.2 Drag 8

I.4 Pressure coefficient 9

I.5 Mach number and the regimes of flight 9

I.6 Incompressible and compressible flow 10

I.7 Dynamic stall phenomenon 11

I.7.1 Description of Dynamic Stall 12

I.7.2 Advantages of dynamic stall 14

I.7.3 The whirling detachment 15

I.7.4 Influence of key parameters on dynamic stall 15

I.8 Leading edge vortices (LEV) 17

Chapter II. Mathematical Formulation 20

II.1 Introduction 20

II.2 Fluid definition 20

II.3 Continuous Media 20

II.4 Instant Navier-Stokes equations 20

II.4.1 Continuity equation 21

II.4.2 Equations of movement quantity [24] 21

II.4.3 Energy equation [24] 21

II.5 Number of Reynolds 23

II.6 The major classes of turbulence modelling 23

II.6.1 Simulation of Navier stokes Averaging Equations (RANS) 24

II.6.2 Direct Numerical Simulation (DNS) 24

II.6.3 Large Eddy Simulation (LES) 24
II.7 Turbulence Models (RANS Approach) 25
II.8 Spalart-Allmaras model 25
II.9 K-ω SST model: 26
II.10 Dynamics: 26
Chapter III. Simulation and results 29
III.1 Static Airfoil 29
III.1.1 Introduction 29
III.1.2 Geometry and Mesh 29
III.1.3 : Results and Discussion 31
III.2 Pitching airfoil 36
III.2.1 Introduction 36
III.2.2 Mesh and Boundary Conditions 36
III.3 Results and Discussion 37
General Conclusion 45

List of figures

Figure I.1: wing planform geometry [2]. 4
Figure I.2: various airfoil shapes [4]. 5
Figure I.3:Airfoil nomenclature [3] 6
Figure I.4: Aerodynamic forces on an airfoil. 7
Figure I.5: Fluid Flow Regimes as a Function of Mach number [6]. 10
Figure I.6: incompressible and compressible flow. 11
Figure I.7: The stages of dynamic stall as shown by Ekaterinaris [16] 13
Figure I.8: MAVs are in a flow regime with very low Reynolds Numbers..... 14
Figure I.9: Vortices generated because of the flow around a flat plate (www.efluids.com). . 15
Figure I.10: CL and CD cycles for different mean impacts (Patersen and al.1998). 16
Figure I.11: CL and CD cycles for different mean impacts (Patersen and al.1998). 17
Figure I.12: Leading edge vortex formation in flapping flight. 18
Figure III.1: the effect of the mesh refinement on the lift coefficient. 30
Figure III.2: Mesh around NACA 0012 airfoil. 30
Figure III.3: Mesh Orthogonal quality. 31
Figure III.4 : Coefficient of Drag versus AOA. 32
Figure III.5: Coefficient of Lift versus AOA. 32
Figure III.6: Comparison of lift coefficient versus angle of attack with the experimental results [24]. 33
Figure III.7: Contours of static pressure at 4° angle of attack. 33
Figure III.8: Contours of static pressure at 8° angle of attack. 34
Figure III.9: Contours of velocity magnitude at 4° angle of attack. 34
Figure III.10: Contours of velocity magnitude at 8° angle of attack. 35
Figure III.11: Contours of velocity magnitude at 14° angle of attack 35
Figure III.12: C- type non-uniform mesh and the zoomed view of the mesh. 36
Figure III.13 Velocity magnitude contours for k=0.1 and x/c = 0.25. 38
Figure III.14: Velocity magnitude contour for k=0.1 and x/c=0.25 at t/T=1.65, enlarged for clarity. 39
Figure III.15: Pressure contours for k=0.1 and x/c = 0.25. 40
Figure III.16: Pressure contour for k=0.1 and x/c=0.25 at t/T=0.7403, enlarged for clarity. 41
Figure III.17: Comparison Coefficient of lift versus AOA and coefficient drag versus AOA for a flapping airfoil with reduced frequency of 0.1 the experimental work. 41

Figure III.18: Comparison of lift coefficient versus angle of attack for all reduced frequencies. 42
Figure III.19: Comparison between static airfoil and pitching airfoil with different reduced frequency values. 43

Introduction

Introduction

Today, new techniques are no longer just human imagination; they are inspired by the creativity of the world around us. This appears very clearly in bionics or robotics. When animals move, their motor organs, shaped by millions of years of evolution, tend to ensure their optimal progression while respecting the constraints of their natural environment. All aircraft and boat builders have to learn from bird watching, fish watching...

Most research on oscillating airfoils or wings is motivated mostly by either a better understanding of animals that use flapping motion for propulsion or the development of micro air vehicles. Also of interest is a better understanding of wing flutter. Wing flutter is of interest for aircraft, helicopters, and turbomachine blades, among others. As is true for most fields within aerodynamics, flapping-wing aerodynamics is a field that benefits from the use of computational fluid dynamics (CFD).

Dynamic stall is a complex fluid dynamics phenomenon of great practical importance. In most cases, this is the first factor to consider when determining the performance of structures exposed to flows. It also appears in aeronautical applications, turbomachinery, and insects. In view of its importance, the literature contains a great deal of work concerning the study of dynamic stall, both with the use of experimental methods and with the application of semi-empirical models or numerical techniques.

The experiment is an indispensable and effective way to predict the characteristics of a flow because it has the advantage of giving the most realistic solution. But this approach requires a very high all from the point of view of time and material means.

A numerical flow simulation is an excellent tool for predicting and studying the physical phenomena governed by the Navier Stokes equations. This technique is very useful in the preliminary design stages. With the numerical approach, it has been possible to quickly model and identify the shapes and configurations for quite complex flow cases, in particular the departures. What made these calculations possible is on the one hand the development of numerical methods for solving fluid mechanics equations and on the other hand the growth of computing capabilities of computers.

The objective of this work is the implementation of a digital model to study the phenomenon of the dynamic stall and to have globular ideas on these aerodynamic phenomena without using the experimental. This study is applied to a NACA0012 profile for an incompressible fluid flow around the profile (NACA0012) in forced oscillations. Preliminary simulations are carried out for a stationary profile placed under different values of the angle of incidence.

In the first chapter: Generalities on flows around an airfoil. An introduction and some different types of wings and airfoils, also the influence of the force on an airfoil, and the main subject the dynamic stall phenomenon.

In the second chapter: Mathematical formulation. Some of Navier-Stockes equations, equations of continuity, movement quantity, and energy.

In the third chapter: simulation and results. The results of the calculations obtained are presented and discussed in this chapter. The first part of this chapter concerns the results obtained in the stationary calculation where the profile is fixed (static airfoil). The second part concerns the results obtained in the simulation of oscillating rotation airfoil.

Finally, we conclude with a general conclusion, and suggestions are made for future research.

.

Chapter I:

Generalities on flows around an airfoil

I.1 Introduction:

The term aero-elasticity is applied to an important class of problems in airplane design. The flexible airframe causes a greater interaction between structural flexibility and aerodynamics. It involves the study of the interaction between aerodynamic forces, elastic forces, inertia forces, and control system dynamics. Such an interaction may be static (such as during a steady level flight or during a trimmed maneuver) or dynamic (involving variations with time) and participation of inertia forces in addition to the elastic, aerodynamic, and control forces in the system dynamic [1].

I.2 Wings and airfoil:

I.2.1 Wing geometry:

The platform of a wing is the shape of the wing seen on a plan view of the aircraft. The figure I.1 illustrates this and includes the names of symbols of the various parameters of the planform geometry. Note that the root ends of the leading and trailing edges have been connected across the fuselage by straight lines. An alternative to this convention is that the leading and trailing edges, if straight, are produced to the aircraft centerline.

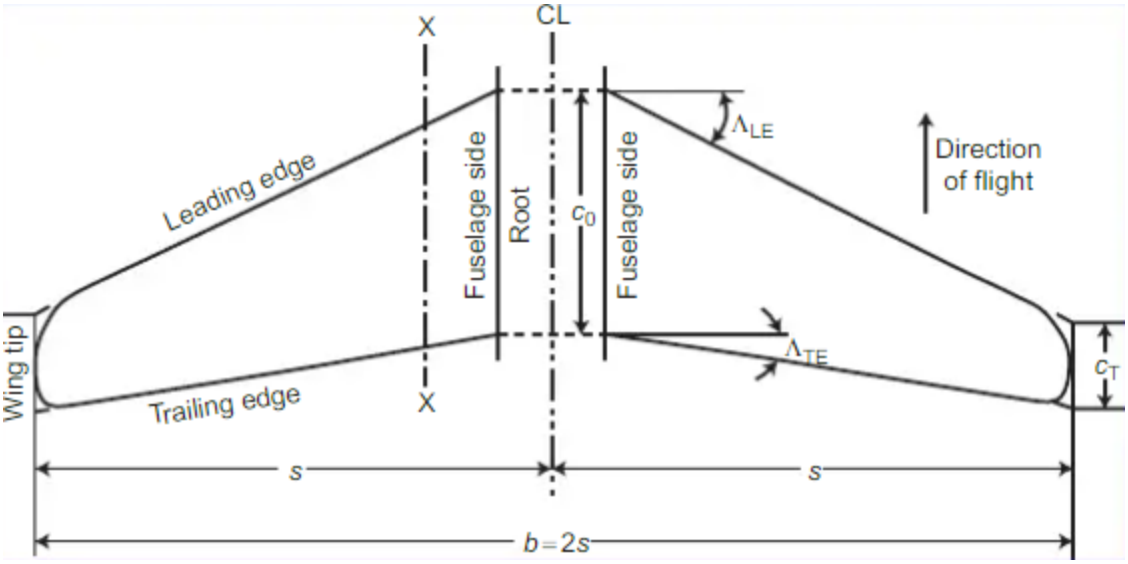

Figure I.1: wing planform geometry [2].

I.2.1.1 Wingspan

The wingspan is the dimension b, the distance between the extreme wingtips. The distance, s, from each tip to the centerline, is the wing semi-span.

I.2.1.2 Wing area

The plan-area of the wing including the continuation within the fuselage is the gross wing area, SG. The unqualified term wing area S is usually intended to mean this gross wing area. The plan-area of the exposed wing, i.e., excluding the continuation within the fuselage, is the net wing area, S_N.

I.2.2 Airfoils

An airfoil shape is a two-dimensional cross-section, parallel to the flow direction, of a three-dimensional wing. While a simple flat plate produces lift when oriented at an angle to the freestream flow, an airfoil section is often designed with curvature and thickness to produce aerodynamic lift more efficiently and effectively.

Airfoil shape is an essential characteristic of a wing and greatly influenced the aerodynamic characteristics and performance of an airplane, the basic airfoil shapes are

I.2.2.1 Symmetric airfoils

Symmetric airfoil has no camber the curvature is identical on both sides compared to the mean line, the chord and camber line are the same. Symmetric airfoil does not produce lift at zero angles of attack.

I.2.2.2 Cambered airfoils

Unlike the symmetric airfoil, a cambered airfoil continues to produce lift for angles of attack zero or even negative thanks to the camber of the airfoil. The more the camber is important the higher the coefficient of lift is large and the angle of attack is smaller critical will be compare to a less cambered airfoil.

I.2.2.3 Supercritical airfoils

A supercritical airfoil is an airfoil that reduces the drag in high subsonic regime, or the airfoil may encounter supersonic flow over parts of the wing.

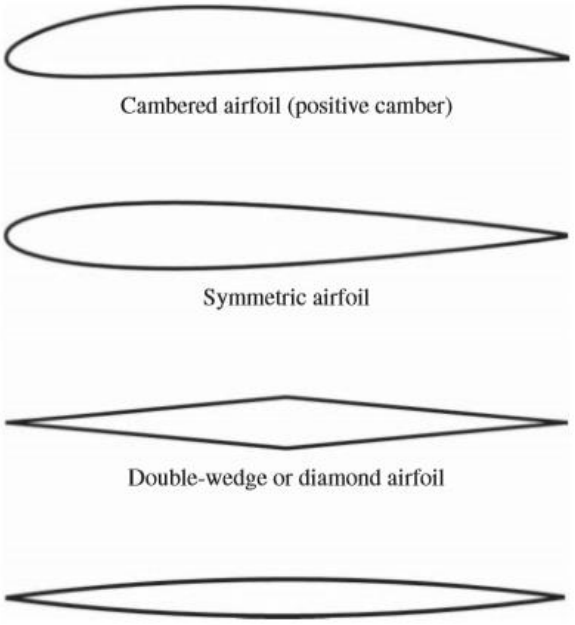

Figure I.2: various airfoil shapes [4].

The geometry of the supercritical airfoil has a reduced curvature in the region of mid-chord of their upper surface, which results in a much higher surface flatter than that of a conventional profile. Camber near the trailing edge of a surface supercritical load bearing is also superior to a conventional airfoil.

I.2.2.4 Supersonic airfoils

Supersonic profiles require different design criteria than those of subsonic profiles to optimize lift in high-speed flight. However, their low-speed characteristics are inferior to subsonic airfoils.

The shape of the bearing surface is designed biconvex (symmetric) of the leading edges angular or very small radius of curvature with a laminar flow section and low thickness/chord with the point of maximum thickness located well behind to produce a favorable pressure gradient over as much of the wing surface as possible, in order to minimize the trail. The double-wedge aerodynamic surfaces (double-wedge airfoil in Figure I.2) are preferred by aircraft, which operate at very high Mach numbers, such as that those researches.

I.2.2.5 Airfoil terminology

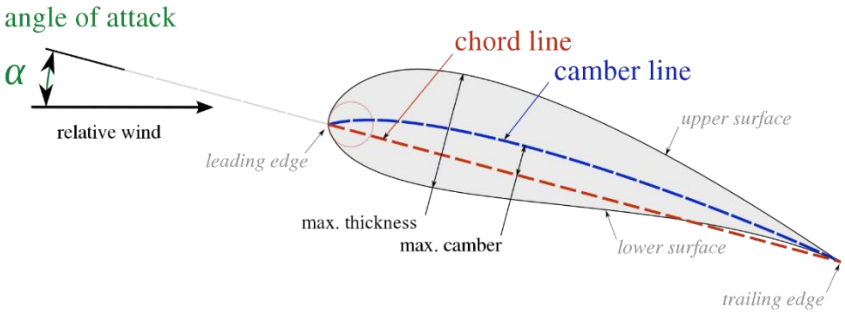

Figure I.3:Airfoil nomenclature [3] .

- **The suction surface** (i.e., the upper surface): is generally associated with higher velocity and thus lower static pressure.
- **The pressure surface** (i.e., the lower surface): has a comparatively higher static pressure than the suction surface. The pressure gradient between these two surfaces contributes to the lift force generated for a given airfoil.
- **The leading edge:** is the point at the front of the airfoil that has maximum curvature.
- **The trailing edge:** is define similarly as the point of maximum curvature at the rear of the airfoil.

- **The chord line:** is a straight line connecting the leading and trailing edges of the airfoil.
- **The chord length**: or simply chord, C, is the length of the chord line and is the characteristic dimension of the airfoil section.
- **The mean camber line:** is the locus of point's midway between the upper and lower surfaces.
- **The aerodynamic center**: is the chord wise length about which the pitching moment, is independent of the lift coefficient and the angle of attack.
- **The center of pressure**: is the chord wise location about which the pitching moment, is zero.

I.3 Aerodynamic Force and Moment

Air flowing past an airplane, or any other body, must be diverted from its original path, and such deflections lead to changes in the speed of the air. Bernoulli's equation shows that the pressure exerted by the air on the airplane is altered from that of the undisturbed stream. In addition, the viscosity of the air leads to the existence of frictional forces tending to resist its flow. Because of these processes, the airplane experiences a resultant aerodynamic force and moment. The lift, drag, and pitching moment are three of the most important of these that we encounter. It is useful to have a non-dimensional form of these aerodynamic forces and moments.

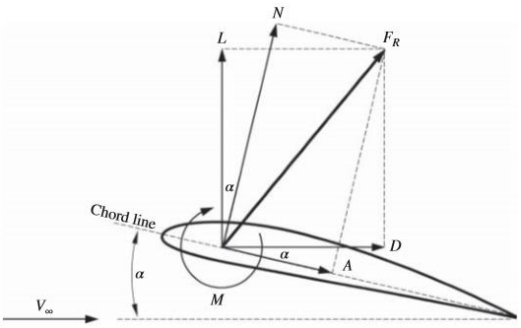

Figure I.4: Aerodynamic forces on an airfoil.

The force coefficient C_F is defined as the aerodynamic force F non-dimensionalized by the freestream dynamic pressure q_∞ multiplied by a reference area S_{ref}, which is typically the wing planform area for an airplane [2].

$$C_F = \frac{F}{q_\infty S_{ref}} = \frac{F}{\frac{1}{2}\rho_\infty V_\infty^2 S_{ref}} = \frac{\text{aerodynamic force}}{\text{dynamic force}} \qquad \text{I–1}$$

Similarly, the moment coefficient is defined as [2]:

$$C_M = \frac{F}{q_\infty c_{ref} S_{ref}} = \frac{F}{\frac{1}{2}\rho_\infty V_\infty^2 c_{ref} S_{ref}} = \frac{\text{aerodynamic moment}}{\text{dynamic moment}} \qquad \text{I–2}$$

Where c_{ref} is the moment reference length, which is typically the wing chord length for an airplane. The non-dimensional aerodynamic coefficients area function of Reynolds number and Mach number, making them particularly useful in comparing different geometries and flows.

I.3.1 Lift

Lift is the component of this force that is perpendicular to the oncoming flow direction. It contrasts with the drag force, which is the component of the force parallel to the flow direction. Lift conventionally acts in an upward direction in order to counter the force of gravity, but it can act in any direction at right angles to the flow [2].

$$L = \frac{1}{2}\rho\, S\, V^2 C_L \qquad \text{I–3}$$

I.3.2 Drag

This is the component of force acting in the opposite direction to the line of flight, or in the same direction as the motion of the undisturbed stream. It is the force that resists the motion of the aircraft. There is no ambiguity regarding its direction or sense [2].

$$D = \frac{1}{2}\rho\, S\, V^2 C_D \qquad \text{I–4}$$

I.4 Pressure coefficient

The pressure acting over the surface area of a body makes an important contribution to the aerodynamic force on the body. The pressure is a dimensional quantity with units of force per unit area, such as N/m2 in SI units and lb/ft2 in English units. We define a dimensionless pressure coefficient as [2]:

$$C_P = \frac{P - P_\infty}{q_\infty} \qquad \text{I–5}$$

Where p is the local pressure, p_∞ is the freestream static pressure, and q_∞ is the freestream dynamic pressure.

I.5 Mach number and the regimes of flight

In fluid dynamics, the Mach number (M or Ma) is a dimensionless quantity representing the ratio of flow velocity past a boundary to the local Sound [4] .The Mach number, M, was defined as the ratio of the airspeed V, to the speed of sound a [5]. Also it is due to the local speed of sound is dependent on the surrounding mediums in specific temperature and pressure.

The Mach number at which an aircraft is flying can be calculated by [5]:

$$\mathrm{M} = \frac{\mathrm{V}}{\mathrm{a}} = \frac{\mathrm{V}}{\sqrt{\gamma \mathrm{RT}}} = \frac{\text{airspeed}}{\text{speed of sound}} \qquad \text{I–6}$$

Table I-1: Classification of flight regimes based on Mach number [2].

Flight regime	Mach number range	Physical flow features
Subsonic	$M < 0.8$	Smoothly changing flow properties Constant density flow (incompressible flow) Acoustic disturbances (sound waves) can propagate upstream
Transonic	$0.8 < M < 1.2$	Subsonic and supersonic flow present Local pocket(s) of supersonic flow, terminating in a shock wave

Supersonic	$1.2 < M < 5$	Shock waves and expansion waves are present in flow Discontinuous flow properties across shock waves Flow density is not constant (compressible flow) Acoustic disturbances (sound waves) cannot propagate upstream
Hypersonic	$M < 5$	Shock waves are closer to a body than for supersonic flow Very high heat transfer High temperature, chemically reacting flows

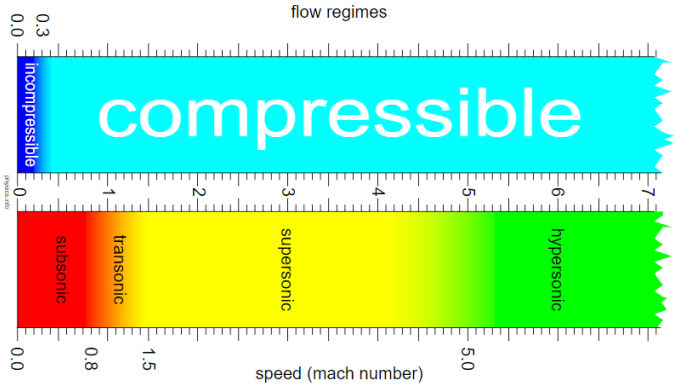

Figure I.5: Fluid Flow Regimes as a Function of Mach number [6].

I.6 Incompressible and compressible flow

Incompressible flow refers to the fluid flow in which the fluid's density is constant. For a density to remain constant, the control volume has to remain constant. Even though the pressure changes, the density will be constant for an incompressible flow. Incompressible flow means flow with variation of density due to pressure changes is negligible or infinitesimal. All the liquids at constant temperature are incompressible.

Compressible flow means a flow that undergoes a notable variation in density with trending pressure. Density ρ (x, y, z) is considered as a field variable for the flow dynamics. When the value of Mach number crosses above 0.3, density begins to vary and the amplitude of variation spikes when Mach number reaches and exceeds unity.

The behavior of control volume (CV) for incompressible and compressible flow is depicted in figure1.6.

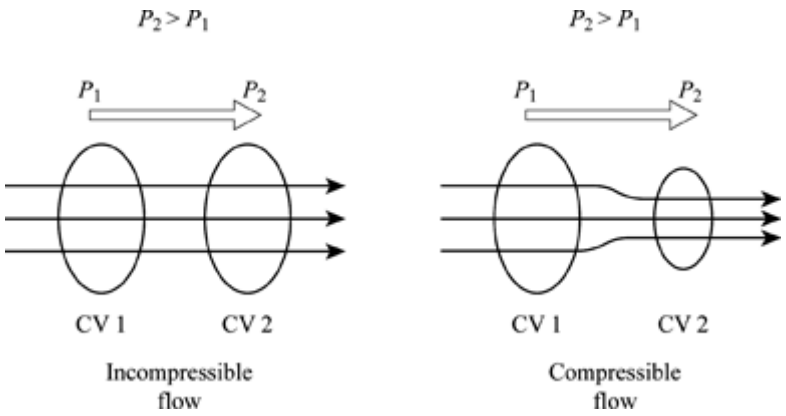

Figure I.6: incompressible and compressible flow.

It can be seen that the CV remains constant for a flow that is incompressible and CV is squeezed for compressible flow.

Bernoulli's equation is applicable only when flow is assumed incompressible. In case of compressible flow, Bernoulli's equation becomes invalid since the very basic assumption for Bernoulli's equation is density ρ is constant [7].

For compressible flow:

$$P + \frac{1}{2}\rho V^2 \neq \text{constant} \qquad \text{I–7}$$

I.7 Dynamic stall phenomenon

Above a certain critical angle of attack, the flow around a load-bearing surface detaches massively and the load-bearing force decreases sharply. This is called a static stall.

The dynamic stall phenomenon is caused by temporal fluctuations in the local angle of fluid incidence on a wing profile. The intensity of this phenomenon imposes on the structures of wind turbines (macs also has other types of rotors such as those of helicopters) constraints that are important for their sizing.

In general, it is possible to define the dynamic stall such as the stall of a wing profile subjected to instantaneous phenomena due to its own movement or to a variation of the upstream flow in the direction of speed. This phenomenon frequently occurs in the case of a wing profile animated by a pitch oscillation movement, particularly when the maximum angle of incidence

exceeds the static stall angle of the profile. Under these conditions, the development of a hysteresis cycle is observed on the drag, lift and pitch coefficients [8].

On a bearing surface with a rapidly increasing incidence, the onset of a stall can be delayed has a significant impact above the critical angle of a static stall. Aerodynamic forces and moments graphically form hysteresis cycles according to the instantaneous incidence $\alpha(t)$. Particularly; the phenomenon is more important if α oscillates around a certain average value α_{mean} which is close to the static stall angle α_s. Stall and its consequences are fundamentally important to the design and operation of aircraft. A certain degree of intentionality always accompanies the flow over a bearing surface or any other fuselage profile has a fairly high angle of attack. But the stall of a load-bearing surface undergoing unstable movement is far more complex than the static stall. Although much progress has been made in recent years, dynamic stall remains a significant unresolved problem with a series of common applications in aeronautics, hydrodynamics, and wind technology [9]. Experiments have shown that dynamic stalling is characterized by the formation and movement of vortices over the upper surface of the supporting surface. This viscous disturbance induces a strongly non-linear pressure fluctuation field. If the frequency, amplitude and maximum incidence are sufficiently high, the phenomenon of vortex detachment is well dispensed [10].

I.7.1 Description of Dynamic Stall

Figure I-7 shows the different stages of the dynamic stall phenomenon [11] [12] .This representation is made by curves of variation of the lift and the moment according to the angle of incidence which correspond to a flow around a profile and what corresponds to this flow by the simplified diagrams (a) a (f):

(a) The beginning of the disbandment of the boundary layer (initially laminar and attached) occurs when the incidence of the profile is greater than the static stall angle. The first recirculation occurs near the trailing edge of the profile on the extrados.

(b) This step corresponds to the onset of the dynamic stall that occurs has a greater impact (approximately 23.4° for NACA profile 0012). The undisturbed portion of the upper surface, estimated at about one third of the rope, undergoes abrupt detachment of the concise boundary accompanied by a depression near the leading edge due to the presence of a massive vortex structure. A vortex appears on the leading edge and moves towards the trailing edge, causing a disorder in the pressure distribution on the upper surface and leading to a stall at the moment.

(c) This is the beginning of the lift stall: the tourbillon generates in (b) passes through the middle of the profit. This gives maximum values of upper-back depression and lift followed by a sudden drop in CL.

(d) Just before the tourbillon escapes, the pitch moment waits for its highest negative value just before the maximum impact. Suddenly the pitch moment goes up sharply while the lift continues to fall.

(e) The tourbillon goes beyond the trailing edge, so completely leaves the profile. The flow is then similar to a flow takes off around a stationary profile. At this stage the hypothesis of secondary vortices is justified by the appearance of pressure peaks the experiments show that the flow takes off and successively recollects near the leading edge.

(f) With the decreasing angle of incidence, the boundary layer gradually recovers on the top of the leading edge to the trailing edge. The values of the aerodynamic loads approach their steady state values and the flow remains attached until the point at which a new cycle begins. Despite the total recollection of the caliche limit at the surface of the profile, the potential external flow remains a little disturbed [13] [14] [15].

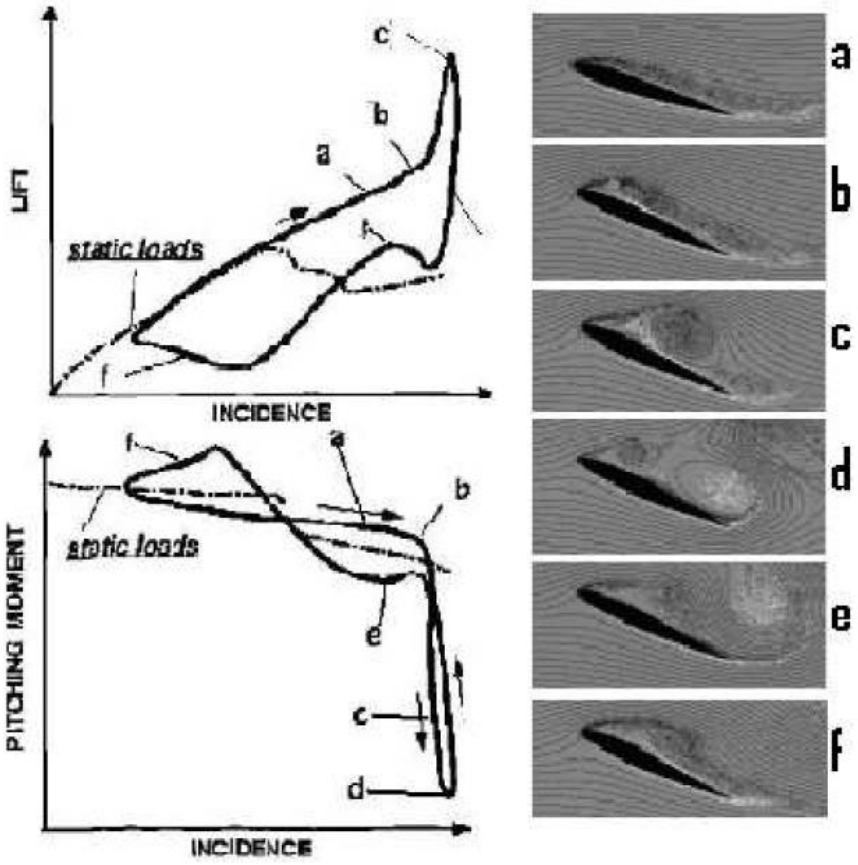

Figure I.7: The stages of dynamic stall as shown by Ekaterinaris [16]

Army has expressed an interest in flapping-wing micro aerial vehicle (MAV) drones [17]. Despite being described as "micro", MAVs typically have a wingspan approximately decimeters. MAVs will fly with a velocity of about 30 to 60 km/h. As seen in Figure 3, their chord Reynolds Number [17]:

$$Re_c = \frac{Uc}{\nu} \qquad \text{I-8}$$

Ranges between 20,000 and 200,000, with large insects on the lower end and small birds on the higher end of this range. Flapping-wing MAVs have an advantage over other types of MAVs (such as fixed-wing or rotary) since they are able to increase their effective Reynolds Number without increasing flight speed [18].

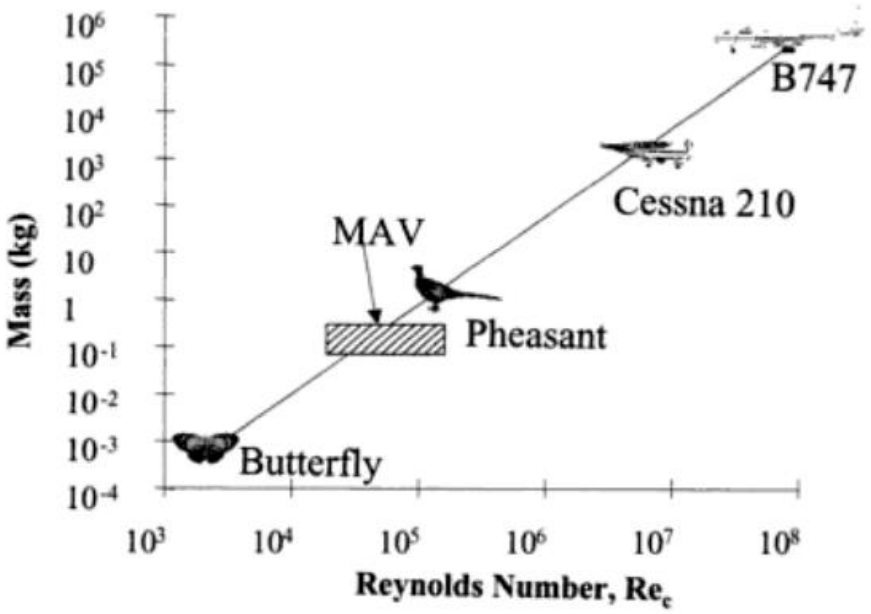

Figure I.8: MAVs are in a flow regime with very low Reynolds Numbers.

I.7.2 Advantages of dynamic stall

On the curve of variation of C_L as a function of the angle of incidence (I-7), we see the representation of the two cases: overlapping around a profile in fixed incidence and the flow around a profile in oscillations. Therefore, we can see that the dynamic stall phenomenon has two advantages: a higher lift and a stall delay (higher stall incidence) compared to the stationary case. This description made the Object of several researchers because of its importance and complexity. For example, the Mc. Croskey [19] report.

I.7.3 The whirling detachment

The existence of a detachment; or of a release of vortices (Figure I-8) downstream of an obstacle placed in a flow, was studied at the beginning of the century by Henri Bénard in France and by Theodor Von Karman in Germany. These vortex flows have been very studied for the circular cylinder.

This is more common for non-profiled obstacles. It depends on the number of Reynolds as it originates within the boundary layer or in the shear layer for angular forms. On angular or curved surfaces, this phenomenon is due to instabilities. For a circular cylinder, there is a spatio-temporal instability of the point of separation of the boundary layer on both sides of the cylinder. When the shapes are angular, the point of detachment is fixed on the edge but the shear layer also undergoes instabilities that induce the activation of the vortices [20].

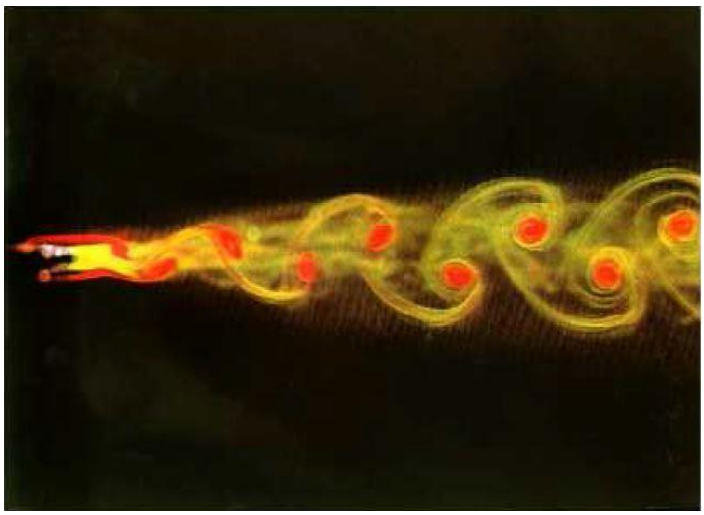

Figure I.9: Vortices generated because of the flow around a flat plate (www.efluids.com).

I.7.4 Influence of key parameters on dynamic stall

The dynamic stall process for a profile can be influenced by many parameters. They can be classified into three types:

- Flow-related parameters such as upstream flow velocity and turbulence rate. Thus, highly developed turbulence will tend to stabilize the boundary layer and delay the development process of dynamic stall.
- Parameters related to the profile: its geometry, its dimensions (rope, span) and its surface condition. The curves representing the variations of the aerodynamic coefficients are different from one profile to another. The results were obtained by

Ramsay et al [21]. show that for the same profile, the cycles of the C_L, C_M and C_D of a smooth surface profile are different from the cycles for a rough surface where the values of C_L, are less important, and the values of C_D are more important.

- Parameters related to the profile movement: the equation of the angle of incidence as a function of time, the frequency of the movement, its amplitude and the mean incidence. Experience shows that hysteresis increases with increasing average incidence angle (Figure I-9) [10].

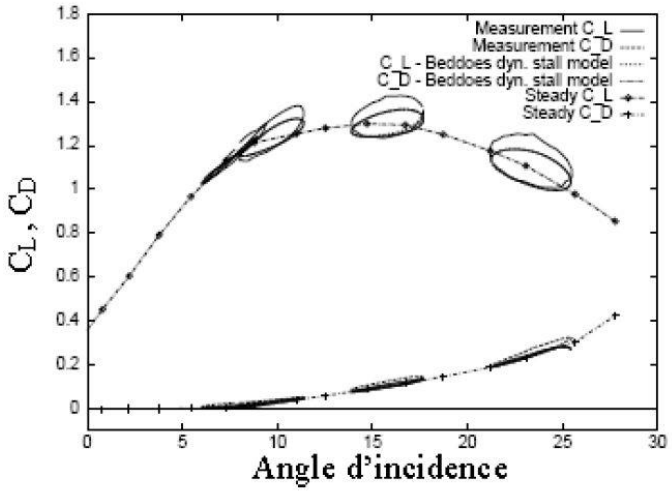

Figure I.10: CL and CD cycles for different mean impacts (Patersen and al.1998).

These parameters are taken into account by the reduced frequency defined by the relationship [10]:

$$k = \frac{c\omega}{2U_\infty}$$

Where c is the profile string,$\omega = 2\pi f$. f is the frequency of motion. Reduced frequency k is the dimensionless number aerodynamics and aero-elasticity; k is one of the parameters that defines the degree of unsteadiness of the problem. This parameter typically corresponds to a relationship between the characteristic convective time scale of the $c/2U$ flow and the characteristic time scale of the movement of the profile (the period of the oscillatory movement). Based on the value of , we can roughly divide the flow into:

- Steady state aerodynamics $k = 0.05$
- Quasi-steady aerodynamics $0 \leq k \leq 0.05$.

- Unsteady aerodynamics $k > 0.05$.

The low values of the reduced frequency correspond to a quasi-stationary flow and the high values at instantaneous flow. In Figure I-10 are shown the cycles of variation of the lift as a function of the angle of incidence of a profile oscillating around 12° and an amplitude of 8° for different values of the reduced frequency, we notice that when we increase the reduced frequency, the cycle becomes wider.

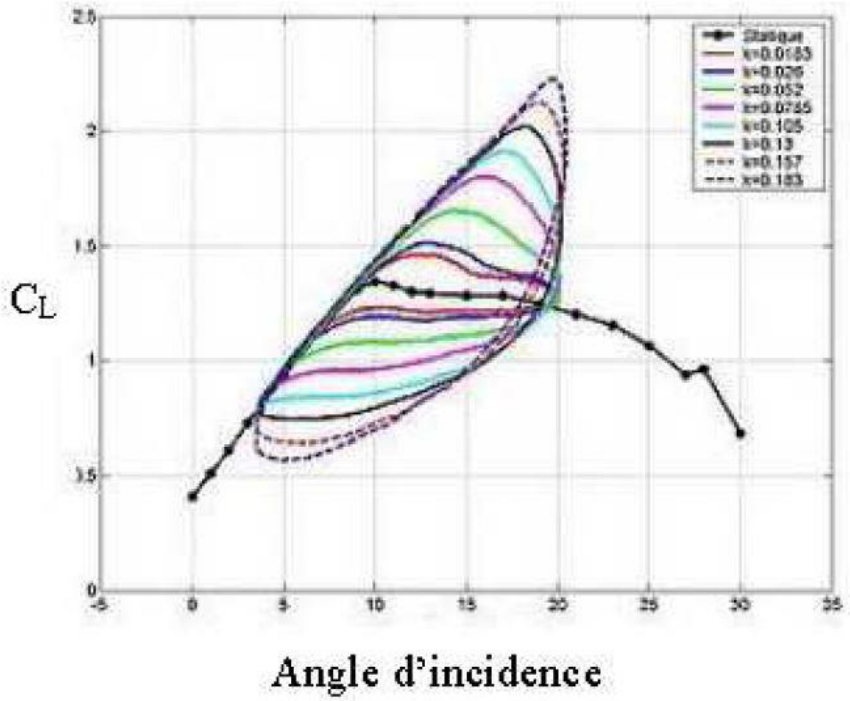

Figure I.11: CL and CD cycles for different mean impacts (Patersen and al.1998).

I.8 Leading edge vortices (LEV)

When the angle of attack or speed of an airfoil is changed, a corresponding amount of vorticity is deposited in the wake. It takes time for the bound vortex to reach its steady state strength when an airfoil is accelerated quickly. The LEV is trapped by the airflow and remains trapped to the upper surface of the wing for several chord-lengths of forward flight, shown in Figure (4). When airflows around the leading edge, it flows over the trapped vortex and is pulled in by the lower pressure generated by the vortex, which in turn generates lift. This mechanism was first discovered by Ellington and at, when they studied the mechanics of forward flight in

bumblebees. The lift enhancing LEV is a main feature during the plunging motion of the stroke [22].

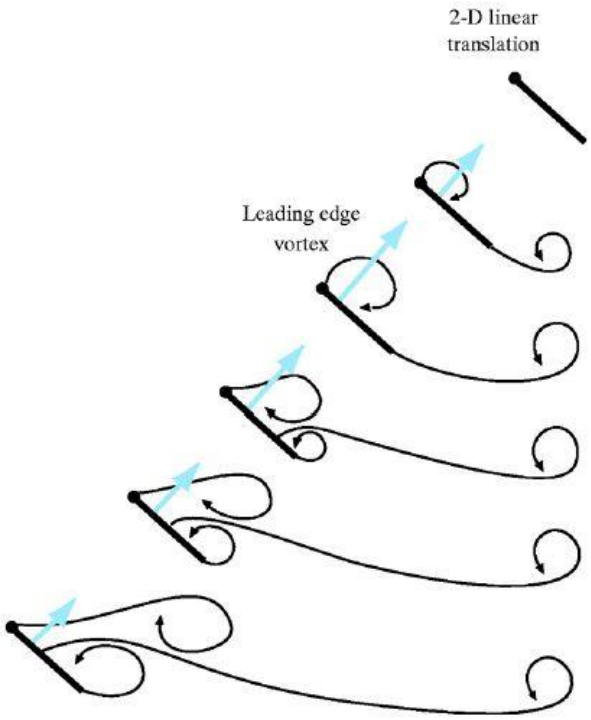

Figure I.12: Leading edge vortex formation in flapping flight.

Chapter II:

Mathematical formulation

II.1 Introduction

In this chapter, we present the mathematical formulation allowing the modelling turbulent viscous flow around a wing profile. The chapter is divided into three parts. In the first, the equations of Navier stokes are recalled. While the second is reserved to recall the different techniques used for the numerical simulation of turbulent flow, finally, one of the techniques based on the RANS approach (Reynolds Averaged Navier Stokes) is the subject of the third part.

II.2 Fluid definition

A fluid represents a continuous medium consisting of a considerable number of infinitely small material particles, which are free to move in relation to each other. The fluid is deformable, without rigidity and it is a medium susceptible to undergo great variations of form under faction forces. We usually draw flows of fluids from the macroscopic point of view by the laws of mechanics of NEWTON, which justifies the name of Newtonian fluids like air and water.

The most important aerodynamic properties of Newtonian fluids support mobility, viscosity and compressibility [23]. Isotropic fluids have identical mechanical properties in all directions of space. A resistance called viscosity accompanies the deformation of the fluid, so we will have a real or viscous fluid. If the viscosity is considered null, we refer to the concept of the perfect fluid. The notion of compressibility, allows to characterize the rate of variation of the density following a pressure variation, in our study, the fluid considered is air, assumes incompressible for small number of Mach ($M \leq 0.3$)

II.3 Continuous Media

A fluid, although composed of atoms at the microscopic level, can be considered at the macroscopic level as a continuous medium: that is, the properties of the fluid are continuous functions of space variables (x,y,z) and time t.

II.4 Instant Navier-Stokes equations

The viscous flow of a fluid, considered as a continuous medium is governed by the Navier-Stokes equation system. The latter are only those which express the variation of the amount of

motion to which we add the equations of mass conservation and energy. Thus, for a flow of viscous, compressible and heat-conducting fluid neglecting the external volume forces (gravity, etc.), these equations are written in the following instantaneous form:

II.4.1 Continuity equation

This equation expresses the principle of mass conservation [24]:

$$\frac{\partial \rho}{\partial t} + \frac{\partial \rho u_j}{\partial x_j} = 0 \qquad \text{II– 1}$$

II.4.2 Equations of movement quantity [24]

$$\frac{\partial \rho u_i}{\partial t} + \frac{\partial}{\partial x_j}\left(\rho u_i u_j + p\delta_{ij}\right) = \frac{\partial \tau_{ij}}{\partial x_j} \qquad \text{II–2}$$

II.4.3 Energy equation [24]

$$\frac{\partial \rho E}{\partial t} + \frac{\partial}{\partial x_j}\left[u_j(\rho E + p)\right] = \frac{\partial}{\partial x_j} u_i - \frac{\partial q_j}{\partial x_j} \qquad \text{II–3}$$

In this system of equations, the total energy per unit of mass is expressed from the internal energy **e** and the kinetic energy according to the relation [24]:

$$E = e + \frac{1}{2} u_k u_k \qquad \text{II–4}$$

In the framework of interest, that is to say for a Newtonian fluid, the tensor τ_{ij} is expressed by the following relation [24]:

$$\tau_{ij} = \mu\left(\frac{\partial u_i}{\partial x_j} + \frac{\partial u_j}{\partial x_i}\right) + \lambda\left(\frac{\partial u_i}{\partial x_j}\right)\delta_{ij} \qquad \text{II–5}$$

According to the Stokes hypothesis, the two coefficients μ and λ are related by the relationship:

$$3\,\lambda + 2\,\mu = 0 \qquad \text{II–6}$$

q_j : Represents the components of the heat stream and is expressed as a function of the

Temperature gradient by Fourier thermal conduction law [24]:

$$q_j = -k\left(\frac{\partial T}{\partial x_j}\right) \qquad \text{II–7}$$

Where k is the thermal conductivity coefficient. This coefficient is expressed as a function of dynamic viscosity using the Prandtl number [24]:

$$\mathrm{P_r} = \frac{\mu c_\mathrm{p}}{k} = \gamma\frac{\mu c_v}{k} \qquad \text{II–8}$$

Where C_p and C_v respectively represent specific heat at pressure and volume Constants and $\gamma = \frac{C_p}{C_v}$

Note that as $\mathrm{e} = \mathrm{C_v}T$, the heat flow can still be expressed in the form [24]:

$$q_j = -\gamma\frac{\mu c_v}{\mathrm{Pr}}\frac{\partial T}{\partial x_j} = -\frac{\gamma\mu}{\mathrm{Pr}}\frac{\partial e}{\partial x_j} \qquad \text{II–9}$$

For air, under standard conditions, the number of Prandtl $\mathrm{P_r}$ is 0.71.

Sutherland's law governs the evolution of dynamic viscosity according to temperature [24].

$$\mu(T) = \mu_0\left(\frac{T}{T_0}\right)^{3/2}\frac{T_0 + 110.4}{T + 110.4} = \frac{1.458 \times 10^{-6}T^{3/2}}{T + 110.4} \qquad \text{II–10}$$

With: $\mathrm{T_0} = 273.15$ K and $\mu_0 = 1.711 \times 10^{-5}$ kg. $\mathrm{m^{-1}\ s^{-1}}$

In order to take into account changes in density and pressure due to temperature variations, the system still requires knowledge of a state law. When considering air as a perfect gas, the equation of state is expressed as [24]:

$$\mathrm{p} = \rho\mathrm{rT} = \rho(\gamma - 1)e \qquad \text{II–11}$$

r Is related to specific heat by Meyer's relation:

$$r = C_p - C_v$$

II.5 Number of Reynolds

The Reynolds Number (Re) is a dimensionless number that characterizes the rocking regime of a fluid around a solid (for example a wing profile). it is defined by:

Reynolds Number = Inertial Force / Viscous Force

This number, related to the relationship between inertia forces and viscosity forces near a body, plays an important role in the subsonic domain where these two types of forces are predominant.

At low Reynolds numbers (low velocities), viscosity forces predominate and flows are called laminar." At high speeds, the importance of inertia forces makes flows "turbulent".

The Reynolds number its physical significance characterizes a flow. In particular the nature of the regime (laminar, transient, turbulent...etc.). It represents the relationship between inertia forces and viscous forces. It is the largest dimensionless number in fluid dynamics [25]

$$R_e = \frac{\rho V L}{\mu}$$

Reynolds number formula is used to determine the velocity, diameter and viscosity of the fluid. The Kind of flow is based on the value of Re

- If Re < 2000, the flow is called Laminar
- If Re > 4000, the flow is called turbulent
- If 2000 < Re < 4000, the flow is called transition.

II.6 The major classes of turbulence modelling

There is no general theory explaining the phenomenon of turbulence but many partial and incomplete theories. Some of these theories, while very rudimentary and very limited, are nevertheless useful for an industrial approach, others more advanced, require more important mathematical developments. There are three main methods of modelling turbulent flow: direct numerical simulation, in which we try to represent the totality of physical phenomena, large scale simulation, in which we represent only the largest vortices as a function of time, and the averaged simulation in which we represent only the average flow.

II.6.1 Simulation of Navier stokes Averaging Equations (RANS)

The RANS (Reynolds averaged Navier stokes) simulations solve the averaged Navier-Stokes's equations. In other words, turbulence is fully modelled here. As a result, the results obtained are not always representative of reality, especially if the simulated configurations are complex. However, this type of simulation makes it possible to obtain a good order of magnitude of the average flow both in terms of speed, temperature or pressure. That is why many of the industrial codes currently on the market are based on this principle. The cost of calculation (in CPU time) is relatively low, which makes it possible to simulate very complex configurations on refined meshes [26].

II.6.2 Direct Numerical Simulation (DNS)

Direct numerical simulation (DNS) simulations are completely opposite to RANS simulations. The Navier-Stokes's equations are fully solved: the turbulence is calculated and no longer modelled. These simulations are therefore very precise but have a cost of calculation far too high for it to be conceivable to simulate an industrial configuration in DNS.

Indeed, the number of points needed to realize a DNS is directly related to the number of Reynolds of the flow ($N = Re^{9/4}$, if the distance between two points adjacent to the mesh is in the order of the Kolmogorov scale).

The results obtained with this kind of simulation are also very useful for creating models that will then be used in LES or RANS. Even if it is not excluded that one day the means of calculation allow such simulations, it is necessary for the next few decades to propose a compromise between the speed of the RANS simulations and the precision of the DNS simulations, this is the large-scale simulation [26].

II.6.3 Large Eddy Simulation (LES)

The LES (Large Eddy Simulation) simulations solve the spatially filtered Navier-Stokes's equations, only the small structures are modelled while all the others are calculated. In practice, spatial filtering is imposed by the mesh: only structures larger than the mesh will be resolved. Moreover, so-called meshed models are introduced to simulate the turbulence of small scales.

With this kind of simulation, it is possible to obtain average but also fluctuating quantities, which is the interest of the LES technique in comparison with the RANS type simulations. The

calculation costs, although higher than for RANS simulations, remain reasonable and allow the simulation of complex geometries on refined meshes.

II.7 Turbulence Models (RANS Approach)

Several turbulence models are available in the ANSYS-FLUENT [27] code, from the zero equation (algebraic) model to the two-equation transport model. The zero-equation model uses algebraic relationships to relate flow fluctuations to the mean variables by using experimental constants. One- and two-equation models use partial differential equations to achieve the same goal. As part of our study, the Spalart-Allmaras model chosen to perform numerical simulations in turbulent flow.

The latter belongs to the so-called "one-equation models" family in which a single partial differential equation is used for the velocity scale, while the length scale is specified algebraically. The velocity scale is typically written in turbulent kinetic energy:

$$k = \frac{1}{2}\left(\overline{u'^2} + \overline{v'^2} + \overline{w'^2}\right) \qquad \text{II–12}$$

k: Turbulent kinetic energy.

Turbulent viscosity is written as suite:

$$\mu_t = \rho k^{1/2} l \qquad \text{II–13}$$

The Spalart-Allmaras (SA) model represents an interesting compromise between zero equation (algebraic) models and two-equation models.

II.8 Spalart-Allmaras model

The Spalart-Allmaras model is a one-equation model. It usually solves a transport equation related to turbulent viscosity μ_t the latter is given for this model by the equation:

$$\mu_t = \rho \widetilde{v} f_{v1} \qquad \text{II–14}$$

μ_t : Turbulent viscosity.

$\tilde{v}$: working variable of the turbulence model.

f_{v1} : Empirical function in the turbulence model.

And the transport equation:

$$\frac{D\tilde{v}}{Dt} = c_{b1}\tilde{S}\tilde{v} + \frac{1}{\sigma}\left[\frac{\partial}{\partial x_j}(v+\tilde{v})\frac{\partial \tilde{v}}{\partial x_j} + c_{b2}\frac{\partial \tilde{v}}{\partial x_j}\frac{\partial \tilde{v}}{\partial x_j}\right] - c_{w1}f_w - \left(\frac{\tilde{U}}{d}\right)^2 \quad \text{II–15}$$

With the constants:

$c_{b1} = 0.1355, \sigma = 2/3$

$c_{b2} = 0.622, k = 0.41$

$c_{w2} = 0.3, c_{w3} = 2$

$c_{w1} = \frac{c_{b1}}{k^2} + \frac{1+c_{b2}}{\sigma}$

The Spalart-Allmaras model requires a refined mesh on the walls, with a value of $y^+ \approx 1$

II.9 K-ω SST model:

This model was proposed by Menter [28] [29], and is derived from a blend of the original k-ω of Wilcox and the standard k-e models. In the inner region, the original k-ω model solved and in the outer region, a gradual switch to the standard k-e model is performed. The idea behind the SST model is to introduce an upper limit for the principal turbulent shear stress in the boundary layers in order to avoid excessive shear-stress levels, typically predicted with Boussineq eddy-viscosity models, and it is able to capture the separation of the flow.

The equation of the dissipation rate specific to turbulence given by:

$$\frac{\partial \rho \mathrm{k}}{\partial t} + \frac{\partial \rho u_j k}{\partial x_j} = P - \beta^* \rho\omega k + \frac{\partial}{\partial x_j}\left((\mu + \sigma_k \mu_t)\frac{\partial \mathrm{k}}{\partial x_j}\right) \quad \text{II–16}$$

$$\frac{\partial \rho \omega}{\partial t} + \frac{\partial \rho u_j \omega}{\partial x_j} = \frac{\gamma}{\nu_t}P - \beta\,\rho\omega^2 + \frac{\partial}{\partial x_j}\left((\mu + \sigma_\omega \mu_t)\frac{\partial \omega}{\partial x_j}\right) + 2(1-F_1)\rho\sigma_{\omega^2}\frac{1}{\omega}\frac{\partial \mathrm{k}}{\partial x_j}\frac{\partial \omega}{\partial x_j} \quad \text{II–17}$$

II.10 Dynamics:

Rival, et. al. [30] suggest the following equation to describe the effective angle of attack undergoing combined pitching and plunging motion.

$$\alpha_{eff}(t) = \alpha_0 + \alpha_1 \cos(2\pi f t + \phi) + \frac{\dot{h}}{U_\infty} + \frac{c\dot{\alpha}}{U_\infty} \qquad \text{II–18}$$

This equation describes the combined pitching and plunging motion. The third term (containing $\dot{h}$, the vertical change in the pitching axis in time) describes the plunging motion and is not relevant for this problem since $\dot{h} = 0$. Rival, et. al [30]. refer to the last term (containing $\dot{\alpha}$, the rate of change of the angle of attack) as dynamic cambering, and find that at low reduced frequencies it may be neglected. The final equation reproduced below.

$$\alpha_{eff}(t) = \alpha_0 + \alpha_1 \sin(\omega t) \qquad \text{II–19}$$

Moreover, reduced frequency (k) is defined to be [25]:

$$k = \frac{\omega c}{2U_\infty} \qquad \text{II–20}$$

Chapter III:

Simulation and results

III.1 Static Airfoil

III.1.1 Introduction

Predetermination of unsteady flow was always a concern for the research because the implementation difficult in laboratories and sophisticated equipment requirements. Our objective of this study is control the simulation of unsteady flows around structures.

For this part, we simulates unsteady flow around a NACA0012 airfoil type in the following condition:

Using the finite volume method and Spalart-Allmars model with Mach number 0.045, pressure101325Pa and the free stream temperature is 300 K, which is the same as the environmental temperature. The density of the air at the given temperature is ρ=1.225kg/m and the viscosity is $\mu=1.7894\times10^{-5}$ kg/m s. Reynolds number is 10.65×10^{5} which the flow can be described as incompressible. A segregated, implicit solver was utilized (ANSYS Fluent) Calculation were done for angles of attack ranging from 0° to 16°.

III.1.2 Geometry and Mesh

The first step in performing a CFD simulation should be to investigate the effect of the mesh size on the solution results. Generally, a numerical solution becomes more accurate as more nodes are used, but using additional nodes also increases the required computer memory and computational time. The appropriate number of nodes can be determined by increasing the number of nodes until the mesh is sufficiently fine so that further refinement does not change the results (Figure III.1).

This study revealed that a C-type grid topology with 40400 quadrilateral cells would be sufficient to establish a grid independent solution (Figure III.2). The domain height was set to approximately 15 chord lengths.

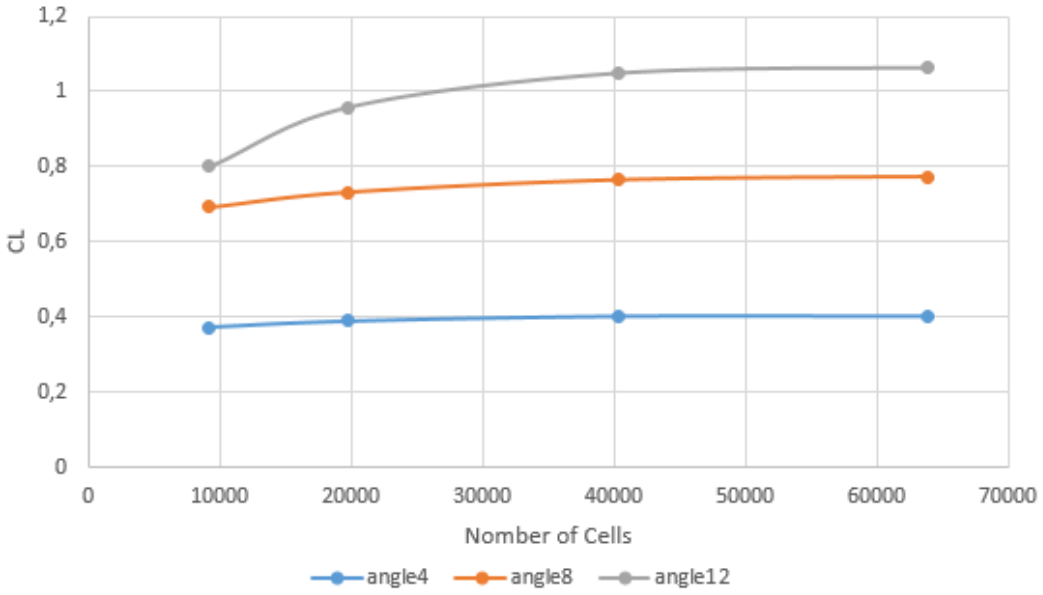

Figure III.1: the effect of the mesh refinement on the lift coefficient.

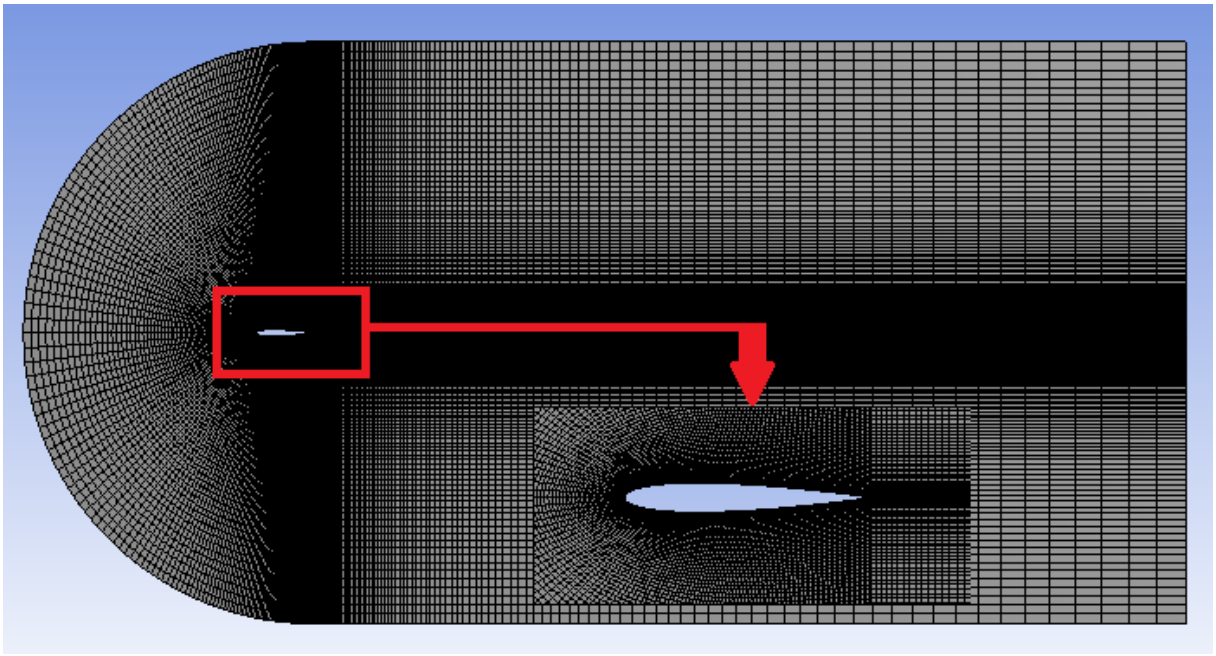

Figure III.2: Mesh around NACA 0012 airfoil.

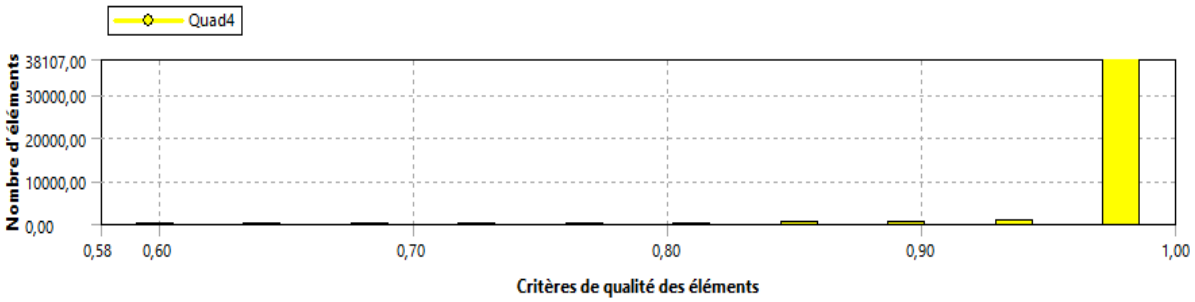

Figure III.3: Mesh Orthogonal quality.

Orthogonal Quality mesh metrics spectrum

Unacceptable	Bad	Acceptable	Good	Very good	Excellent
0-0.001	0.001-0.14	0.15-0.20	0.20-0.69	0.70-0.95	0.95-1.00

Table III-1: Orthogonal Quality Mesh [31].

Low orthogonal values or high inclinations are not recommended. In general, an attempt is made to maintain a minimum orthogonal quality > 0.1, or a maximum inclination of 0.95. However, these values may differ depending on the physics and location of the cell. A good mesh quality means that:

- ✓ The mesh quality criteria are in the correct range - Orthogonal quality.
- ✓ The mesh size is valid for the studied physics - Boundary layer.
- ✓ Important geometric details are well captured.

III.1.3 : Results and Discussion

On an airfoil, the resultants of the forces are usually resolved into two forces and one moment. The component of the net force acting normal to the incoming flow stream known as the lift force and the component of the net force acting parallel to the incoming flow stream known as the drag force. The curves of the lift and the drag coefficient shown for various angles of attack from 0° to 16°.

Aerodynamic Characteristics at Re 10.65×10^5 can be observed from the Drag coefficient, which is shown in (Figure III.4) continuous to increase as the angle of attack, increases gradually. The maximum drag coefficient is around 0.197 at 16° angle of attack. The lift coefficient, which shown in (Figure III.5), also increases gradually as the angle of attack is increase from 0° to 14° but it starts decrease right after that angle. The maximum lift coefficient achieved for this airfoil is about 1.136 at 14° angle of attack.

The current work results were compared with the experimental CL2 [24] and the results of lift coefficient are coincide well with the experimental results (Figure III.6).

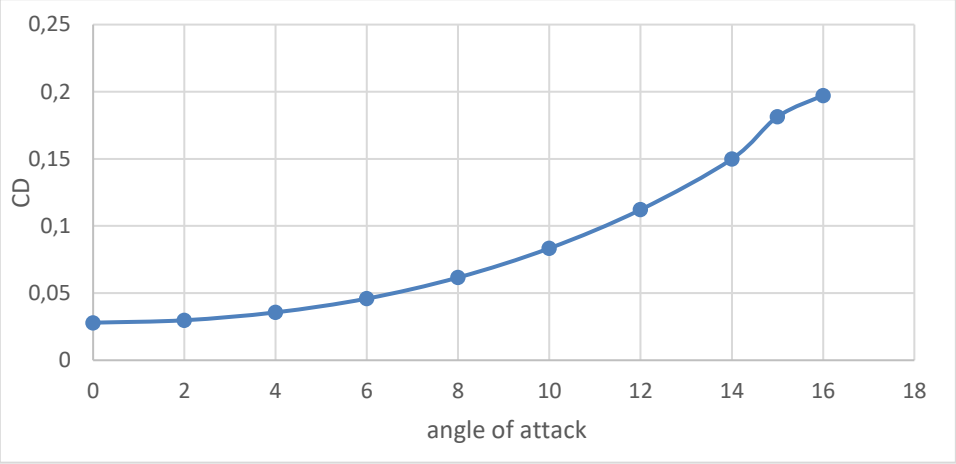

Figure III.4 : Coefficient of Drag versus AOA.

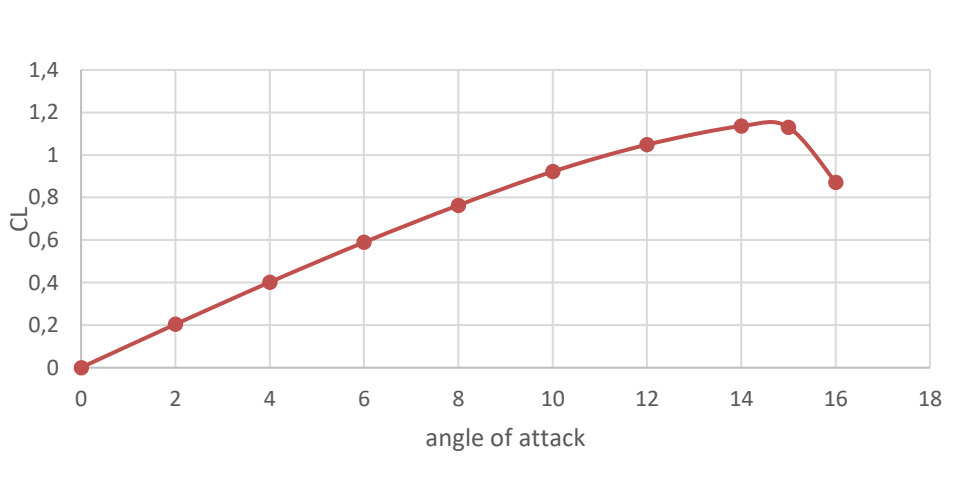

Figure III.5: Coefficient of Lift versus AOA.

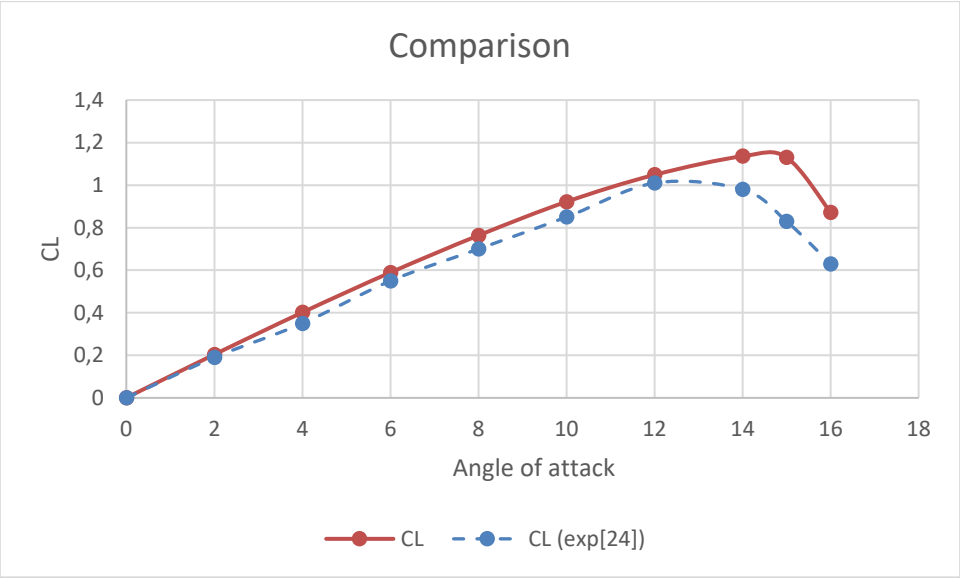

Figure III.6: Comparison of lift coefficient versus angle of attack with the experimental results [24].

Figures III.7 and III.8 shows the simulation outcomes of static pressure at angles of attack 4 and 8° with the Spalart-Allmaras turbulence model. The pressure on the lower surface of the airfoil was greater than that of the incoming.

Flow stream and as a result, it effectively “pushed” the airfoil upward, normal to the incoming flow stream. On the other hand, the components of the pressure distribution parallel to the incoming flow stream tended to slow the velocity of the incoming flow relative to the airfoil, as do the viscous stresses.

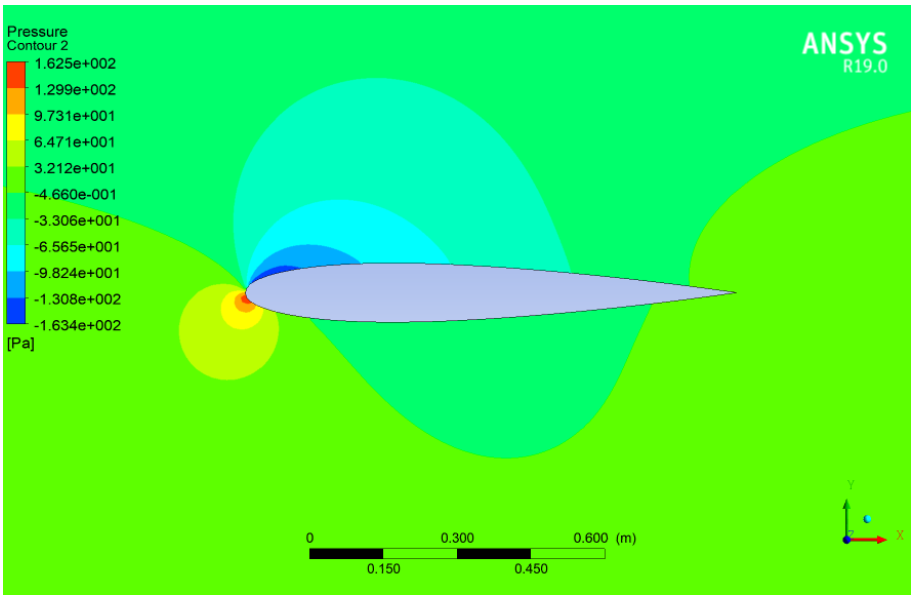

Figure III.7: Contours of static pressure at 4° angle of attack.

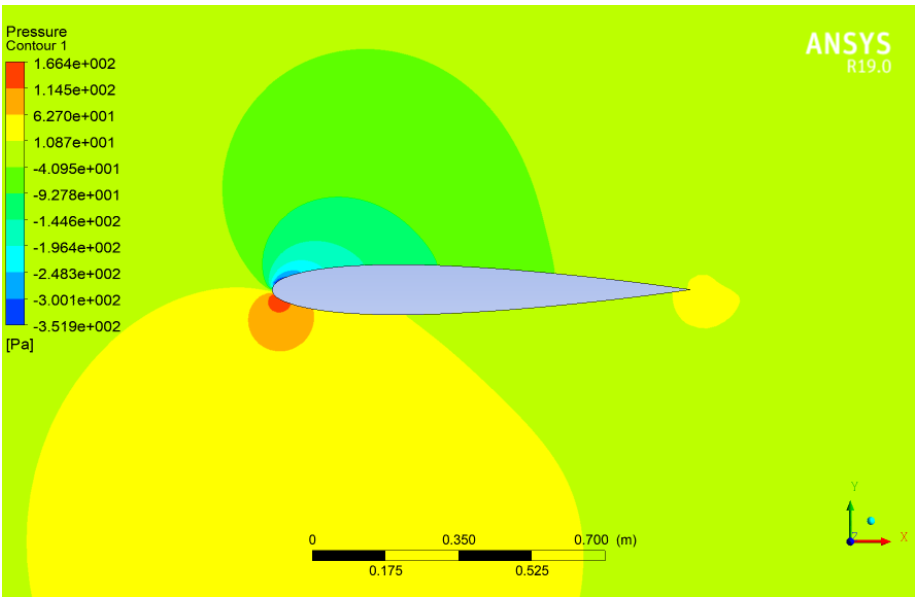

Figure III.8: Contours of static pressure at 8° angle of attack.

Contours of velocity components at angles of attack 4, 8, and 14° are also shown (Figures III.9, 10, and 11). The trailing edge stagnation point moved slightly forward on the airfoil at low angles of attack and it jumped rapidly to leading edge at stall angle. A stagnation point is a point in a flow field where the local velocity of the fluid is zero. The upper surface of the airfoil experienced a higher velocity compared to the lower surface. That was expected from the pressure distribution. As the angle of attack increased the upper surface, velocity was much high than the velocity of the lower surface.

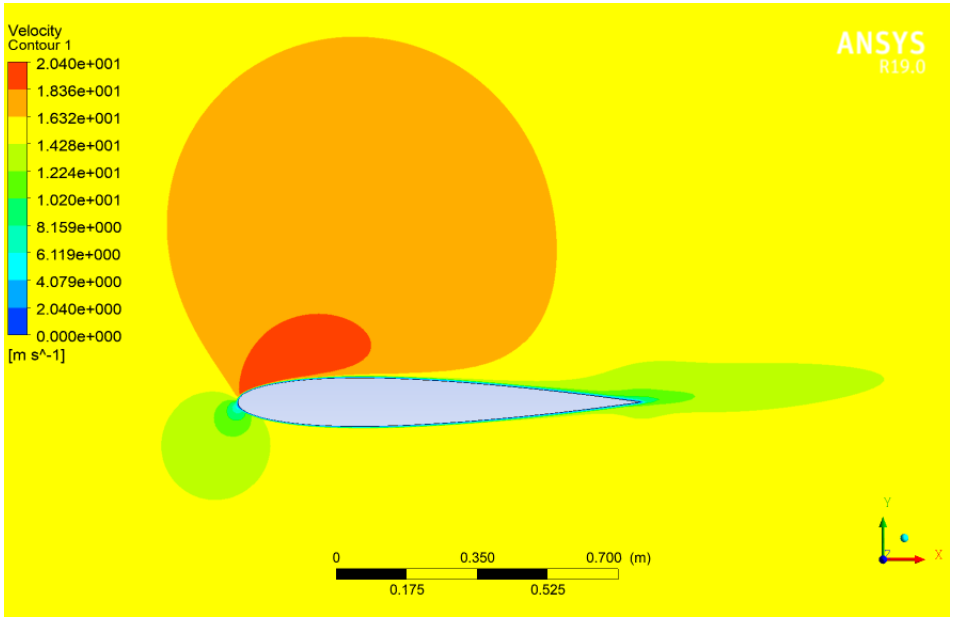

Figure III.9: Contours of velocity magnitude at 4° angle of attack.

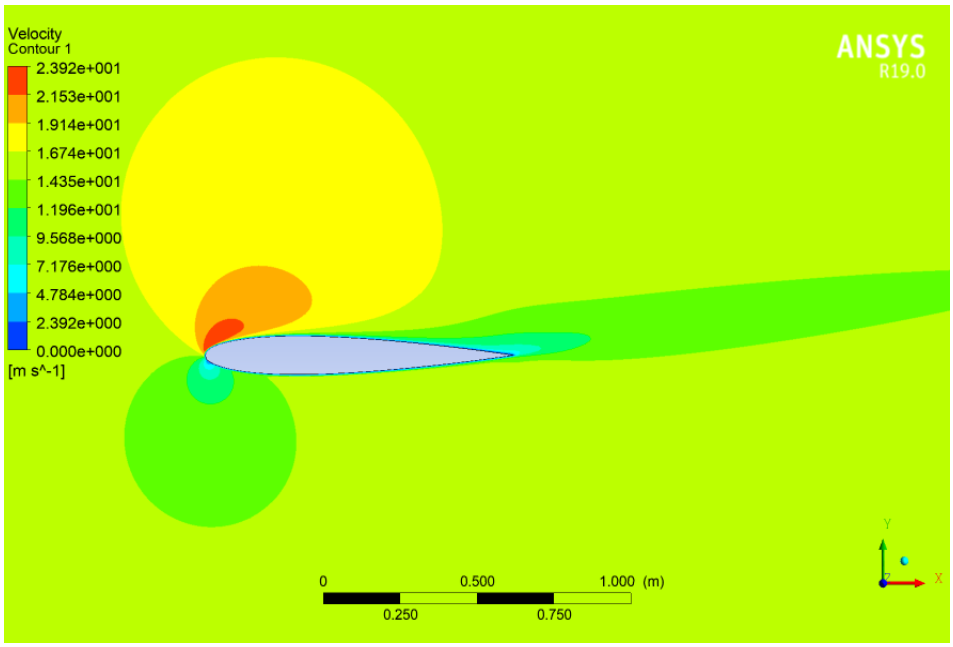

Figure III.10: Contours of velocity magnitude at 8° angle of attack.

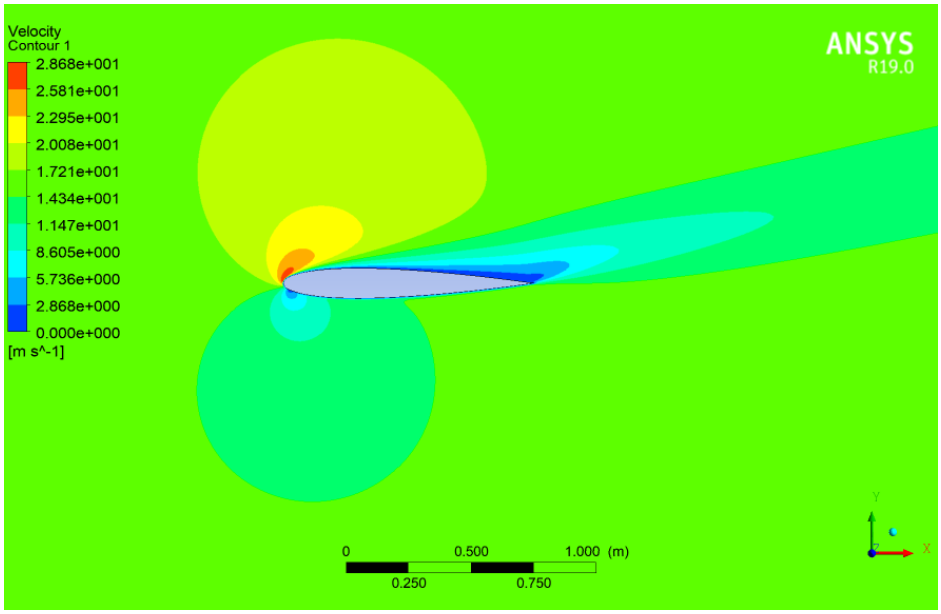

Figure III.11: Contours of velocity magnitude at 14° angle of attack

III.2 Pitching airfoil

III.2.1 Introduction

For this part we consider the NACA 0012 flapping airfoil with a chord length of c=1m, that undergoes sinusoidal Pitching motion with an angle of attack of $\alpha=0°+20°\sin(\omega t)$. The center of rotation is 0.25 from the leading edge. The reduced frequencies of the airfoil are ($\kappa=\omega c/2U\infty$) of 0.1, 0.2 and 0.3. The physical oscillating frequency is varied with a range of an angular velocity (ω) range of 3.112 rad/s to 9.34 rad/s respectively. The chord Reynolds number is 10.65×10^5 with the freestream velocity ($U\infty$) of 15.56 m/s by using K-ω SST model.

III.2.2 Mesh and Boundary Conditions

The velocity inlet is placed at 5 chord lengths upstream from the airfoil and the pressure outlet is placed at 20 chord lengths downstream from the airfoil. Figure III.12 shows the grid with computational domain and the zoomed view of the mesh. We used a non-uniform C-Type fine mesh with 40400. The time step for this study is 0.01 s. For mesh convergence test, reduced frequency of 0.1 was adopted with the large enough computational domain. The initial angle of attack was set to 0°.The transient incompressible solver from OpenFOAM 8.0 was used and PIMPLE algorithm was adopted for velocity-pressure coupling. We used the finite volume-based solver in which the solution is calculated on each control volume. For a flapping airfoil, the above said combinations are important to see the good accuracy in the results. We used our own solver in OpenFOAM to solve the problem and integrated the solver in PimpleDyMFoam (scillatingRotatingMotion).It is an implementation of PimpleFoam that automatically allows the dynamic meshes. The dynamic mesh automatically modifies the grid points i.e., squeezing and stretching the cells, according to an unsteady motion.

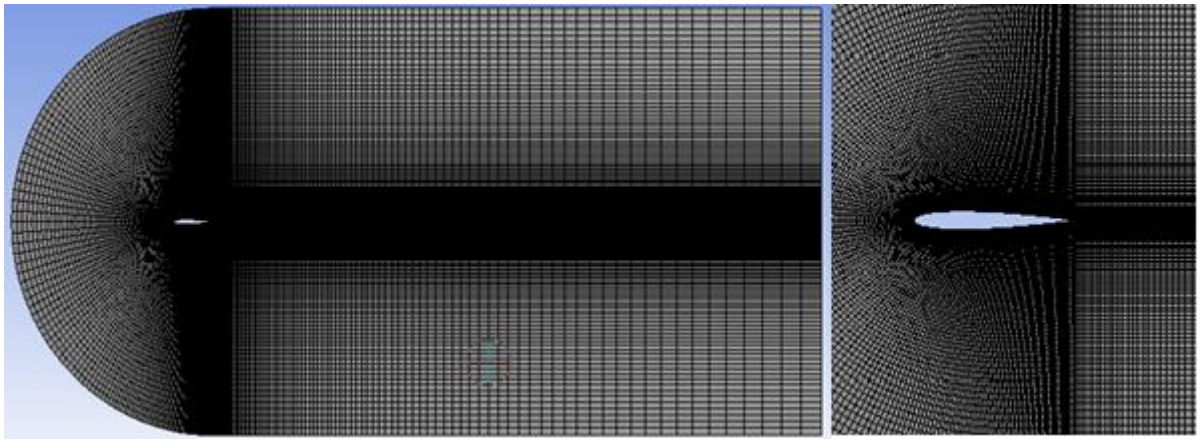

Figure III.12: C- type non-uniform mesh and the zoomed view of the mesh.

III.3 Results and Discussion

For the results reported here, the free-stream velocity was approximately U∞ =15.56 cm/sec, resulting in a chord Reynolds number of 10.65×10^5 and a reduced frequency of k = 0.1 (f /Hz). The mean angle of attack was set to zero so that the angle of attack of the airfoil varied between -20 and 20, 20 being the amplitude of pitch waveform. The flow field does not qualitatively change appreciably from case to case, so results presented here are from the case with a reduced frequency of 0.1 and a pitching axis located at the quarter-chord of the airfoil. Figure 15 shows velocity magnitude contours from a full period of motion of the case with a reduced frequency of 0.1 and a pitch axis location of 0.25c.

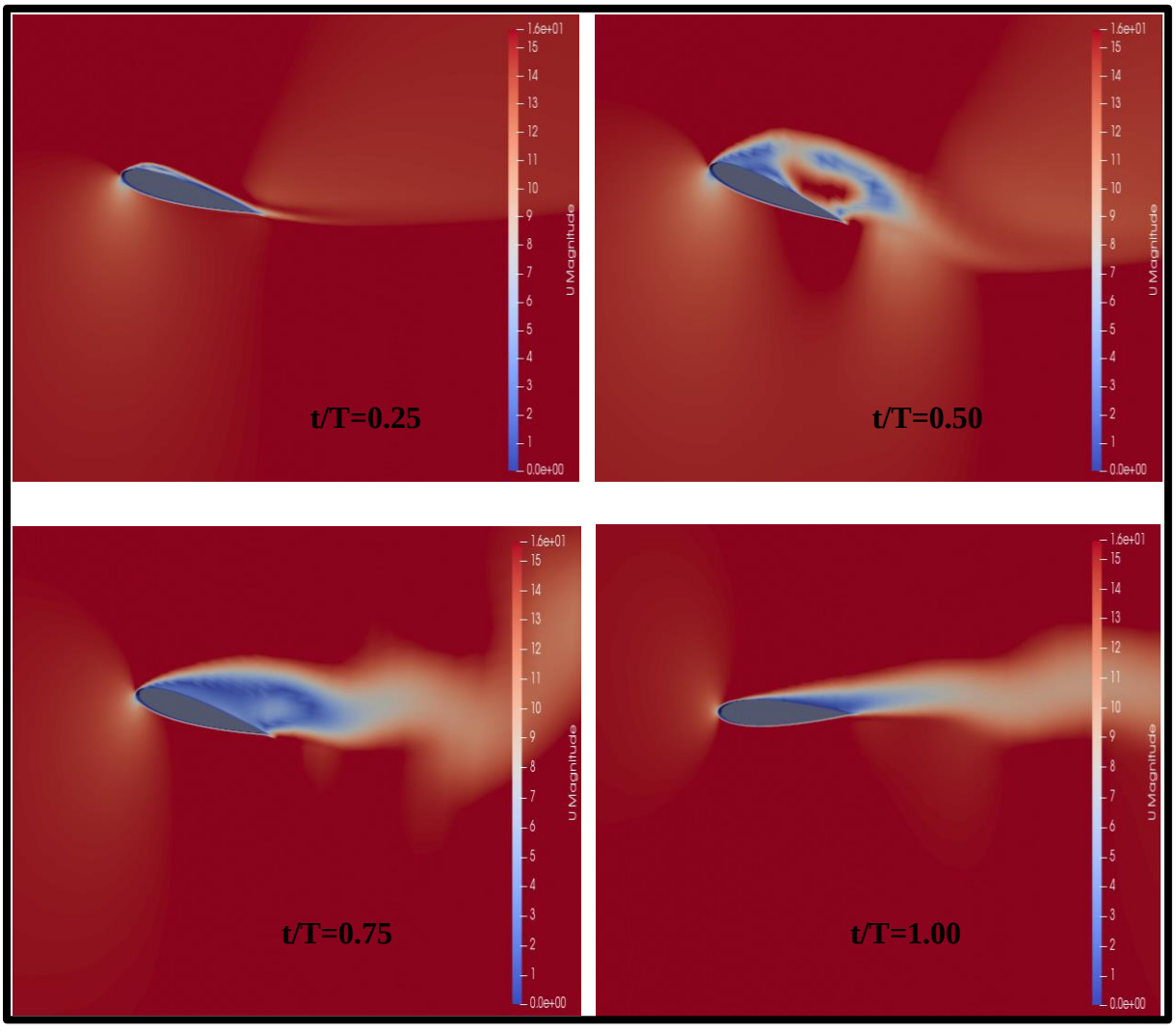

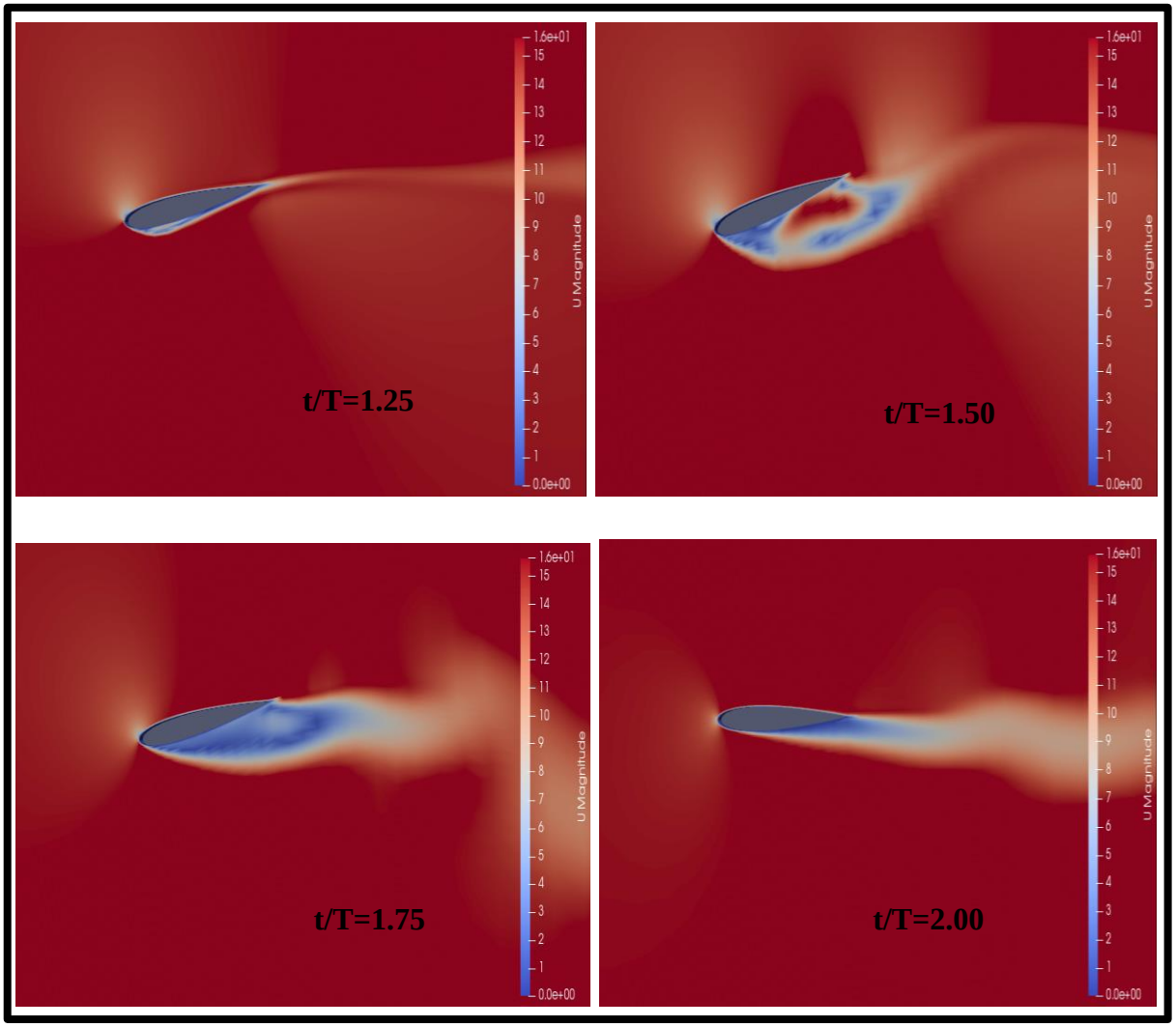

Figure III.13 Velocity magnitude contours for k=0.1 and x/c = 0.25.

The first three images of Figure III.13 show the first upstroke (trailing edge moving upwards) of a period and therefore include the stall from the previous period. At this point the angle of attack is approximately 20° and decreasing. Once the angle of attack is sufficiently low (approaching the minimum 0°) the flow reattaches. This is seen at time 1.00. At this point the airfoil starts a downstroke (trailing edge moving downwards) and therefore the angle of attack is increasing. As the angle of attack approaches the static stall angle at time 1.25, a leading edge vortex is shed. This vortex continues down the chord of the airfoil until it passes the trailing edge at time 1.50. It is during this time that the spike in lift occurs, the angle of attack reaches the maximum -20°, and the airfoil once again begins an upstroke (the trailing edge is moving upwards and the angle of attack is decreasing). Once the vortex is sufficiently far from the airfoil, the flow separates and enters deep stall. Figure III.14 shows time 1.65 enlarged for clarity.

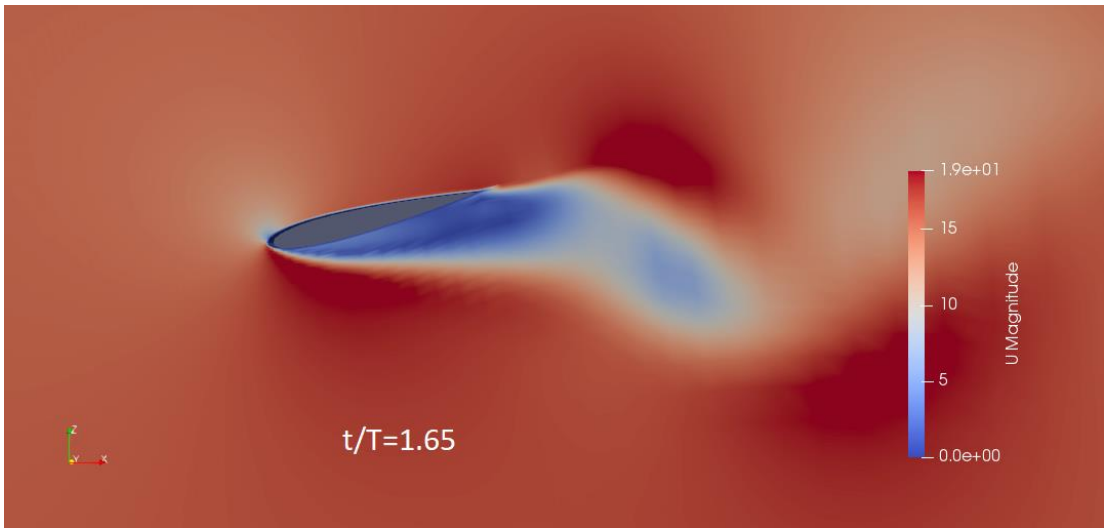

Figure III.14: Velocity magnitude contour for k=0.1 and x/c=0.25 at t/T=1.65, enlarged for clarity.

The pressure varies over an entire period as velocity does, so Figure III.15 shows the pressure field varying over one period. Results presented here are from the case with a reduced frequency of 0.1 and a pitching axis located at the quarter chord. The second image of Figure III.15 shows a low-pressure region directly over the trailing edge and is an artifact from the previous oscillation. When the flow is attached as indicated by Figure III.13 (t/T = 0.25), the pressure contours show a high pressure on the lower surface of the airfoil and a low-pressure region on the upper surface. Once the leading-edge vortex is shed (t/T = 1.25), the pressure contours indicate that the low-pressure region on the upper surface of the airfoil, previously restricted to near the leading edge, has expanded to the entire upper surface. This is what causes the lift spikes. Once the flow separates and enters a deep stall, the pressure contours reflect this – the pressure on the upper surface is much higher and the pressure on the lower surface is much lower. Figure III.16 shows time 1.65 enlarged for clarity.

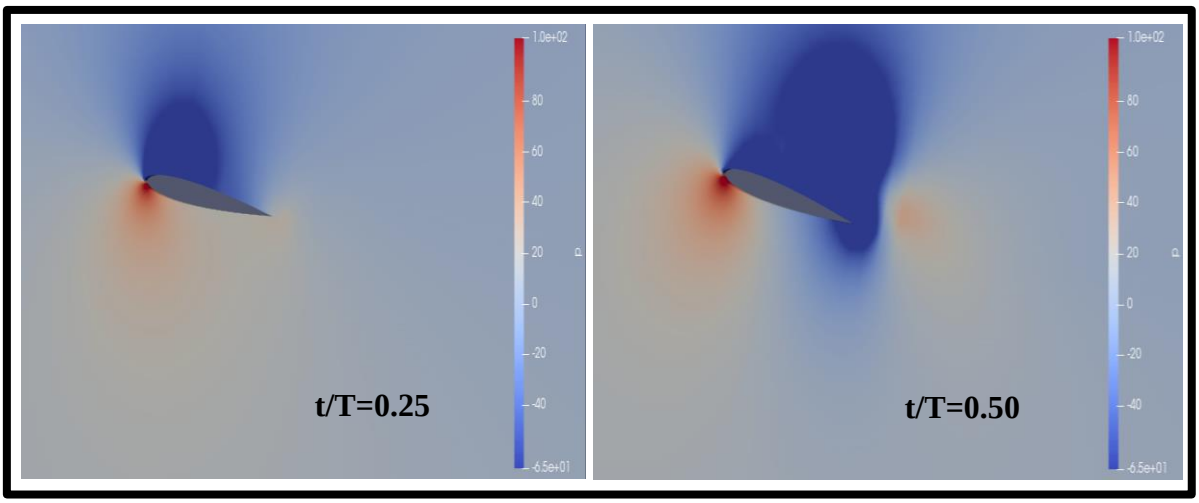

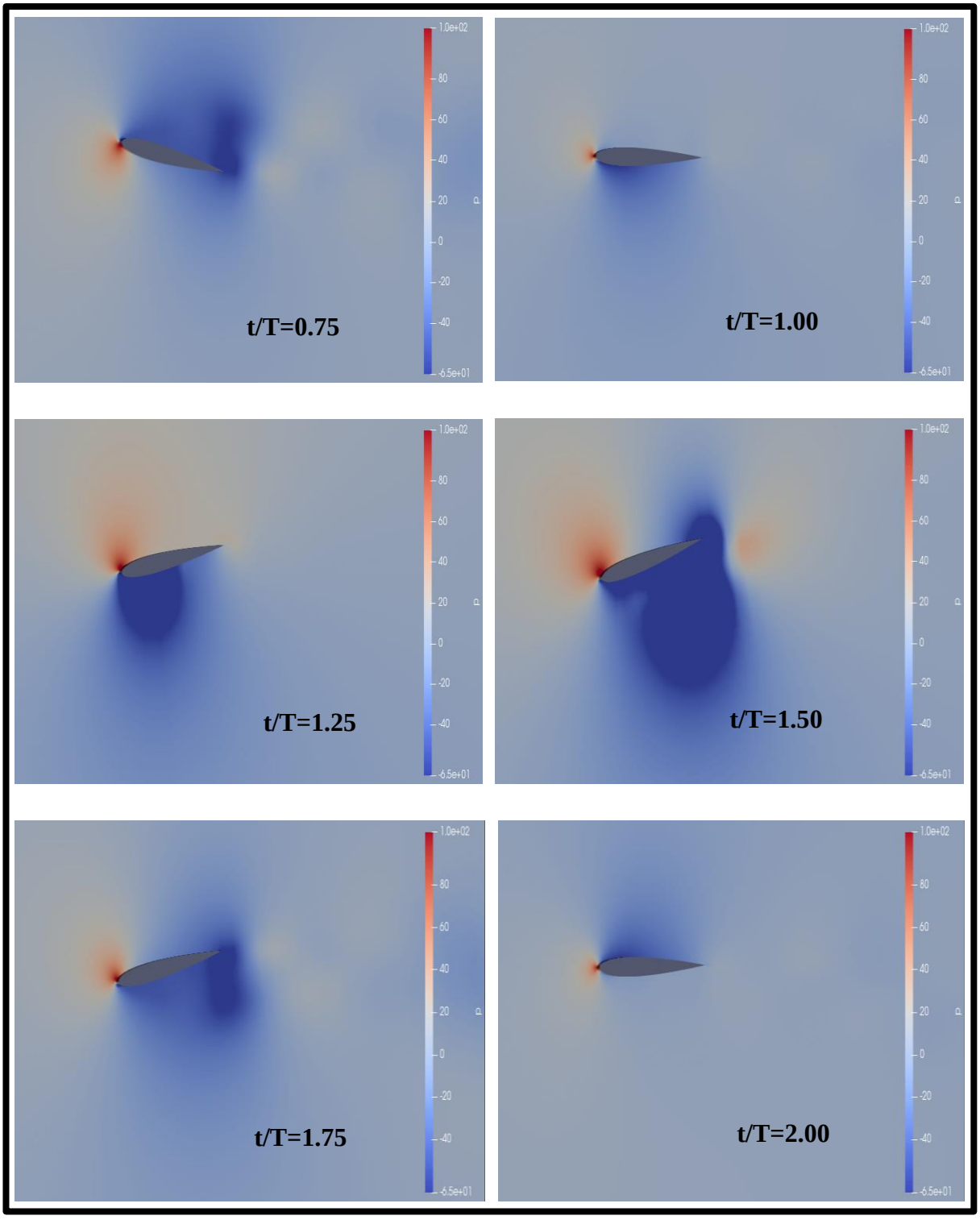

Figure III.15: Pressure contours for k=0.1 and x/c = 0.25.

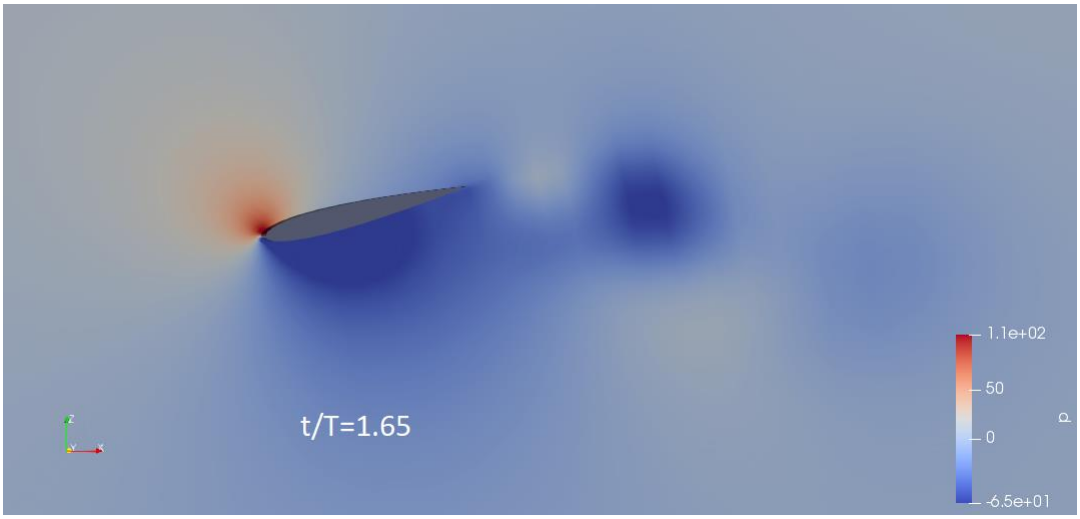

Figure III.16: Pressure contour for k=0.1 and x/c=0.25 at t/T=0.7403, enlarged for clarity.

FigureIII.17 .depicts the validation of coefficient of lift versus angle of attack and coefficient of drag versus angle of attack with the experimental work for a flapping airfoil actuation at reduced frequency of 0.1. The maximum lift coefficient with reduced frequency of 0.1 is 1.61, whereas the maximum drag coefficient is 0.43. The present work results are closely followed the trend of the experimental work [32]. It was important to note that the difference between the present OpenFOAM work and experimental works tended to decrease as reduced frequency decreased.

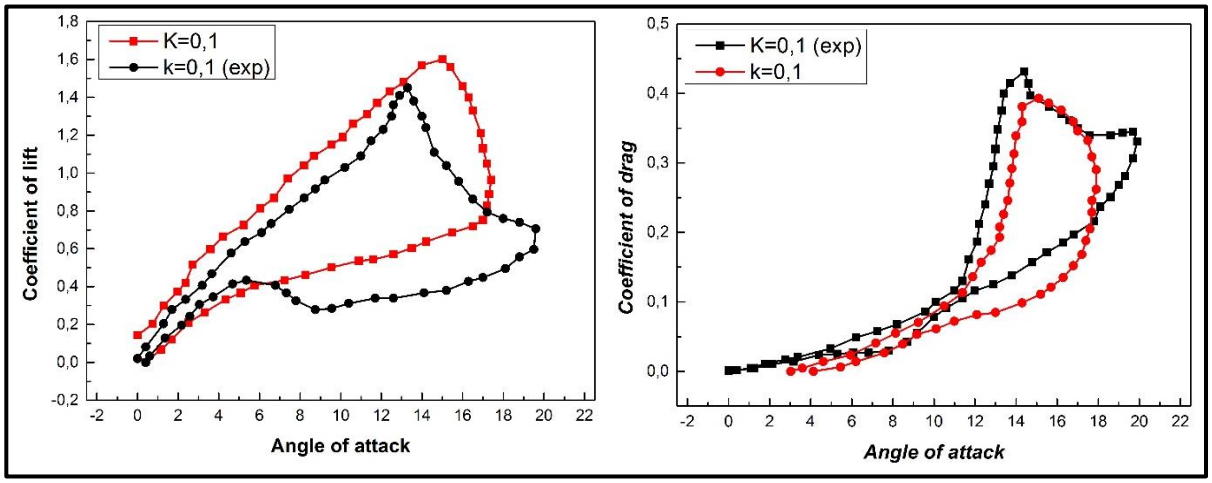

Figure III.17: Comparison Coefficient of lift versus AOA and coefficient drag versus AOA for a flapping airfoil with reduced frequency of 0.1 the experimental work.

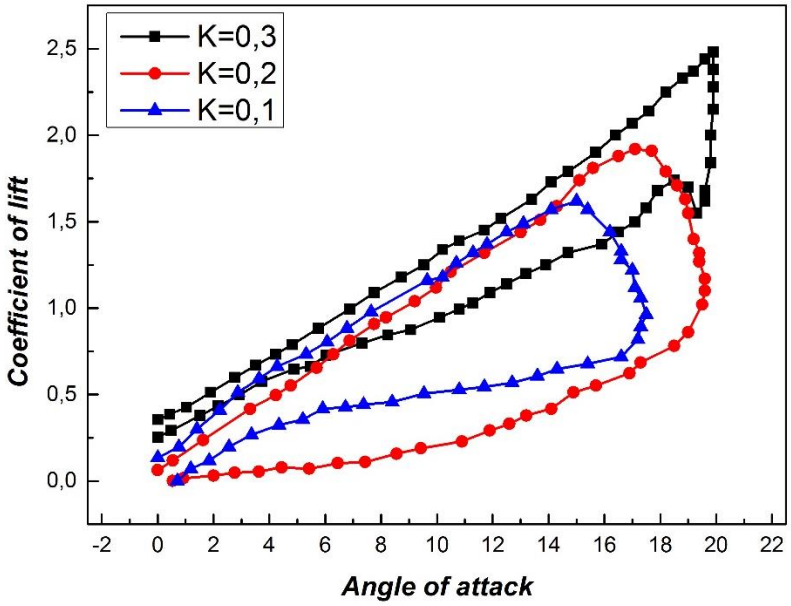

Figure III.18: Comparison of lift coefficient versus angle of attack for all reduced frequencies.

Figure.III.18 presents the effect of the reduced frequency at 0.3 is dominant than the other reduced frequencies. The reduced frequency is unsteady parameter, which ensures the significant positive effect on a flapping airfoil because of the angular velocities. When a flapping airfoil moves up and down with some angle, the angular velocities plays an important role. From the observation the reduced frequency of the flapping airfoil at 0.1, 0.2 and 0.3 showed the maximum lift coefficient of 1.61, 1.91, and 2.44 respectively. We have observed that the effect of reduced frequency is beneficial and positive at all the values. For unsteady aerodynamics, the consideration of the reduced frequency is important. The combination of the reduced frequency actuation over a flapping airfoil gave the extra lift generation, drag reduction, and dynamic stall angle delay.

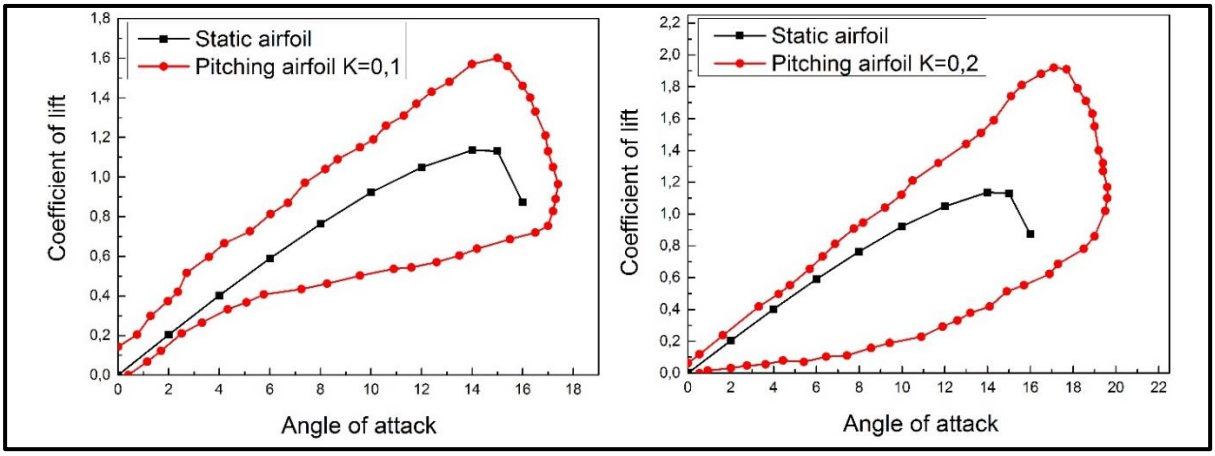

Figure III.19: Comparison between static airfoil and pitching airfoil with different reduced frequency values.

Figure III.19 shown that at pitching motion the lift coefficient is greater than the static airfoil with the same angle of attack. Also, by using a different value of reduced frequency in the pitching motion we observed that there is an extra lift generation in addition to dynamic stall angle delay compared to static airfoil results.

General conclusion

General Conclusion

This thesis has shown the influence of the angle of attack, pitch motion and the reduced frequency on the aerodynamic properties (specifically lift and drag) of a NACA 0012 airfoil undergoing pitching oscillations at a Reynolds number of 10.65×10^5. Workbench19.0 and OpenFOAM 8.0 are the CFD solvers. Fluent and Paraview (specifically paraFoam – an OpenFOAM utility) are used in post-processing to view the solution. Excel and Origin were used to create graphs and data plots.

Results show that by pitching the airfoil about a mean nonzero angle of attack and causing it to dynamically stall, it is possible to achieve a lift coefficient (average and maximum) that is greater than that of a static airfoil at the same mean angle of attack.

In general, increasing the reduced frequency causes the maximum and average lift coefficients to increase. A greater reduced frequency may yet produce thrust, but high-reduced frequencies tend to generate chaotic behavior in the system.

Among the future perspectives our studies and simulations can be continued with a plunging motion and pitching+plunging simulations

This study may be improved in a number of ways. Even though 2D CFD is capable of capturing the dynamic stall phenomenon, it is inherently a 3D problem, so a 3D grid would be better suited for this problem. Large eddy simulations (LES) or detached eddy simulations (DES) would provide better accuracy and show better formation of the vortices shed, but due to limited computational resources, this thesis used a RANS approach.

Références

[1] P. Chinmaya and S. Venkatasubramani , “eroelasticity- In General and Flutter Phenomenon,” *Engineering and Industrial Services TATA Consultancy Services Limited,* no. 978-0-7695-3884-6/09, 2009.

[2] H. E.L. and C. P.W, Aerodynamics for Engineering Students, LONDON , 2003 .

[3] [Online]. Available: http://www.esru.strath.ac.uk/EandE/Web_sites/11-12/MORE/hydrofoil/introduction.html.

[4] c. stephen, “INTRODUCTION TO AEROSPACE ENGINEERING WITH A FLIGHT TEST PERSPECTIVE,” John Wiley & Sons Ltd, United Kingdom, 2017.

[5] l. aymen, “what is the much numbre,” *what is the much numbre,* no. 337632133, 2019.

[6] [Online]. Available: https://physics.info/turbulence/#:~:text=Fluid%20flow%20can%20be%20broken,are%20said%20to%20be%20supersonic%20.&text=Mach%20numbers%20between%200.8%20and%201.5%20are%20said%20to%20be%20transonic%20.

[7] [Online]. Available: https://www.chegg.com/homework-help/definitions/incompressible-and-compressible-flow-5.

[8] Analyse physique et modélisation d'écoulement instationnaires turbulents autour de prols oscil lants et d'éoliennes., France: PhD thesis, Institut Na-tional Polytechnique de Toulouse, 2007.

[9] M. C. W.J., “the phenomenon of dynamic stall,” Technical raport ames research center , USA, 1981.

[10] A. BEKHTI, Simulation de l'écoulement autour d'un profil d'aile en ocillation forcées Application aux rotor éoliens, Mémoire de magistere , 2009-2010.

[11] “A new stall onset criterion for low speed dynamic stall,” no. 4 :461471,, 2006.

[12] P. K. Gee, “Wind turbine load prediction using the beddoes-leishman model for unsteady aerodynamic and dynamic stall,” Master's thesis,University of Utah,, 1996.

[13] k. O.Y and S. G.M, “calculation od dynamic stall on an oscillating arifoil,” no. 41 :452-455, 2000.

[14] J.Szidlowsky, “Simulation numerique de l'ecoulement autour en configuration de décrochage dynamique,” PhD thesis Université d'Orléans, 2006.

[15] C. T. and J. Smith, “Analysis of low-speed unsteady airfoil flows,” Springer ans Horizons Publishing, 2008.

[16] J. A. Ekaterinaris and M. F. Platzer, Computational Prediction of Airfoil Dynamic, Prog. Aerospace Sci, 1997).

[17] J. Judsen,, “Flappable,” Army Studying Wing Technology For Unmanned Aerial, 16 March 2012 Accessed 22 May 2012.

[18] Mueller,, T and al, “fixed and Flapping Wing Aerodynamics for Micro Air,” Progress in Astronautics and Aeronautics, 2001.

[19] M. C. W,J, “Unsteady airfoil,” Ann, Rev fluid Mesh 14;285-311, 1982.

[20] H. P, “Vibration couplées avec le vent,” Technical raport, Ecole polytechnique, Palaiseau, 2004.

[21] R. R. R, H. M.J and G. G.M, “Effect of grit roughness and pitch oscollation on th s809 airfoil,” Technical report , Ohio state University , 1995.

[22] . O. Marten, “Effects of wing gusts on rigid flapping NACA 0012 airfoil at Re=3000,” Aerodynamic of insect flight, 2015.

[23] B. Allan and L. James , AÉRODYNAMIQUE THÉORIES DE LA DYNAMIQUE DES FLUIDES, 1989.

[24] N. Bekka, “Numerical Study of Heat Transfer Around the Small Scale Airfoil Using Various Turbulence Models,” no. 10.1080/10407780903508005, 11 Jan 2010.

[25] B.Boukhemla and O.Douaissia, “Simulation numérique de l'ecoulement autour d'un profil oscillant,” Projet de fin d'etude, 2008/2009.

[26] F. V, Etude expérimental et numérique du controle actif de jets dans des chambres de combustion, thèse de doctorat à l'institut national polytechnique de Toulouse, 2003.

[27] D. A.M and R. M.F, “Experimental investigation into the aerodynamic properties of a flexible and rigid wing micro air vehicle,” Portloand, Oregan, 28 june-1 july 2004.

[28] M. F. R. and R. L. C. , Assessment of Two-Equation Turbulence Models for Transonic Flows, 1994..

[29] H. H. M. , K. R. , K. M and M. H, Calculation of Steady and Pulsating Impinging jets—An Assessment of 13 Widely Used Turbulence Models, Numer. Heat Transfer B, vol. 51, no, 6, pp, 2007.

[30] Rival D and Tropea C, “Characteristics of Pitching and Plunging Airfoils Under Dynamic-Stall Conditions,” January-February 2010.

[31] ANSYS, “Mesh Quality & Advanced Topics,” Introduction to ANSYS Meshing, © 2015 ANSYS, Inc., February 12, 2015.

[32] T. a. G. P. Lee, “Investigation of Flow Over an Oscillating Airfoil,” no. 512, pp.313–341, 2004.

[33] C. Dave and H. Chad, “Aerodynamic Flutter,” Carol D. Weiseman, NASA Langley Research Center .

[34] [Online]. Available: http://engineeringisabell.weebly.com/principles-of-flight-2.html.

[35] [Online]. Available: https://www.researchgate.net/figure/The-von-Karman-vortex-street-generated-by-the-Rishiri-island-of-Hokkaido-Japan-top_fig1_331768849.

[36] F. A, “Equations Statistique des gaz turbulent,” Comptes Rendus de l'Académie des sciences 246, 1956.

Annex

NACA 0012:

Upper surface		Lower surface	
X cord	Y cord	X cord	Y cord
1.0000	0.0000	0.0039	-0.0109
0.9961	0.0006	0.0157	-0.0211
0.9843	0.0023	0.0351	-0.0305
0.9649	0.0050	0.0618	-0.0389
0.9382	0.0086	0.0955	-0.0460
0.9045	0.0131	0.1355	-0.0519
0.8645	0.0181	0.1813	-0.0562
0.8187	0.0236	0.2321	-0.0589
0.7679	0.0293	0.2871	-0.0600
0.7129	0.0350	0.3455	-0.0596
0.6545	0.0407	0.4063	-0.0578
0.5937	0.0460	0.4686	-0.0547
0.5314	0.0508	0.5314	-0.0508
0.4686	0.0547	0.5937	-0.0460
0.4063	0.0578	0.6545	-0.0407
0.3455	0.0596	0.7129	-0.0350
0.2871	0.0600	0.7679	-0.0293
0.2321	0.0589	0.8187	-0.0236
0.1813	0.0562	0.8645	-0.0181
0.1355	0.0519	0.9045	-0.0131
0.0955	0.0460	0.9382	-0.0086
0.0618	0.0389	0.9649	-0.0050
0.0351	0.0305	0.9843	-0.0023
0.0157	0.0211	0.9961	-0.0006
0.0039	0.0109		
0.0000	0.0000		

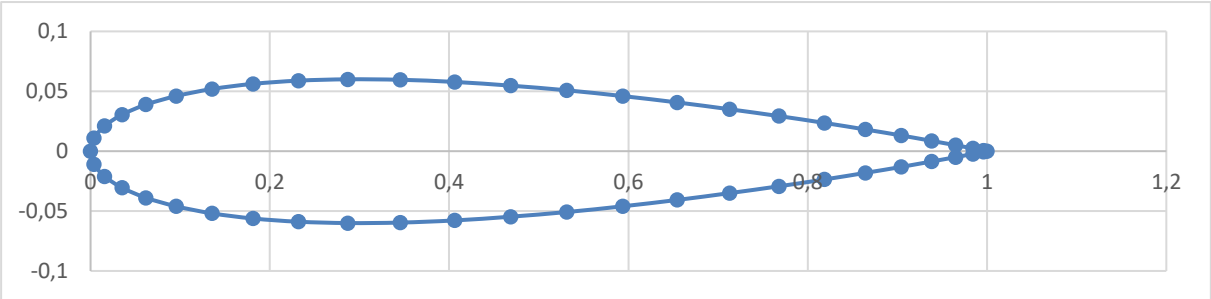

Figure A.1: NACA0012 airfoil.

OpenFoam

OpenFOAM (Open Field Operations and Manipulations) is an open source collection of numerical solvers and utilities. There are solvers for laminar and turbulent flow, compressible and incompressible flow, transient and steady-state flow, static and dynamic meshes. It includes solvers for solid mechanics (solving displacement equations) and financial modeling (solving the Black-Scholes equation for pricing stock options). The solver chosen for this thesis is the pimpleDyMFoam solver. This solver accepts turbulence models (though turbulence can also be turned off), is transient, incompressible, and allows for a dynamic mesh. OpenFOAM also has many preprocessing and post processing utilities. The general format for an OpenFOAM case (depicted in Figure A.2) is simply a directory named for that case. The case directory will contain three folders: the constant folder, the system folder, and the 0 folder. The constant folder contains information about the properties of the fluid, turbulence, geometry, and mesh. The system folder contains information that controls the solver such as starting and ending times, timesteps, maximum courant numbers, and finite volume schemes to use to solve the discretized sets of equations. The 0 folder contains the initial and boundary conditions of the flow and geometric properties and additional time folders are generated upon running the solver based on the writing frequency defined in the system directory. OpenFOAM has a reliable error handing system that will alert the user if any of these files are missing or are not formatted properly.

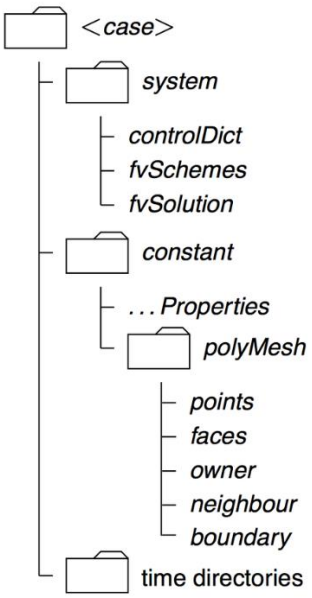

Figure A.2: General format for OpenFOAM cases (as shown on the OpenFOAM website)

OpenFoam case folders

dynamicMeshDict:

```
FoamFile
{
    version     2.0;
    format      ascii;
    class       dictionary;
    object      dynamicMeshDict;
}
// * * * * * * * * * * * * * * * * * * * * * * * * * * * * * * * * * * * * * * * * * * * * //

dynamicFvMesh      dynamicMotionSolverFvMesh;

motionSolverLibs ("libfvMotionSolvers.so");

solver    interpolatingSolidBody;

solidBodyMotionFunction oscillatingRotatingMotion;


patches         (aerofoil);
CofG            (0.25 0 0);

innerDistance   0.01;
outerDistance   4.0;

oscillatingRotatingMotionCoeffs
{
   origin          (0.25 0 0);
   amplitude       (0 20 0);
   omega           3.112;
}

// ************************************************************************* //
```

initialConditions:

```
FoamFile
{
    version     2.0;
    format      ascii;
    class       IOobject;
    location    "0";
    object      initialConditions;
}
// * * * * * * * * * * * * * * * * * * * * * * * * * * * * * * * * * * * * * * * * * * * * //

// simulation controls

np                          4; // number of processors for parallel computation
iterations                  2; // total number of iterations (to be increases, see NOTES below)
writeEvery               1e-2; // writes down step data every "writeEvery" iterations

// airfoil properties

alpha                       0; // deg - incidence angle
chord                       1; // chord length
CR                  (0.25 0 0); // center of rotation
pitch               (0 1 0); // pitch axis direction

// fluid properties

mach                    0.045;
Rair                   287.05; // J / (Kg*K)
gamma                     1.4;
Tref                      300; // K
muVal                1.82e-05; // dynamic viscosity
rhoVal                    1.17; // must be consistent with rho = R*T/P (see fields in 0.orig)

// turbulence properties

turbModel          kOmegaSST;
hWall                0.01106; // firt cell height Compute as: hWall = Hz / SUM( i from 0 to Nz-1 )( zGrading ^ (i / (Nz-1)) )
```

- Run simulation by BlueCFD-core 2020 terminal:
  - ✓ BlockMesh
  - ✓ decomposePar
  - ✓ mpirun –np 4 pimpleFoam –parallel
  - ✓ reconstructPar
  - ✓ FoamToVTK
  - ✓ Paraview

Paraview